PHOTON CORRELATION SPECTROSCOPY STUDIES OF MUTUAL DIFFUSION IN AQUEOUS t-BUTYL ALCOHOL

by

GARY W. EULISS

B.S., Southwest Missouri State University, 1980

A MASTER'S THESIS

submitted in partial fulfillment of the

requirements for the degree

MASTER OF SCIENCE

Department of Physics

KANSAS STATE UNIVERSITY

Manhattan, Kansas

1983

Approved:

Major Professor

TABLE OF CONTENTS

LIST OF FIGURES

LIST OF TABLES

THIS BOOK
CONTAINS
NUMEROUS PAGES
WITH THE ORIGINAL
PRINTING BEING
SKEWED
DIFFERENTLY FROM
THE TOP OF THE
PAGE TO THE
BOTTOM.

THIS IS AS RECEIVED
FROM THE
CUSTOMER.

ACKNOWLEDGEMENTS

I first want to thank my parents. The accomplishments I have made would not have been possible without the love, support, and words of encouragement which they have given me.

Next, I would like to thank Chris Sorensen for his advice and instruction. I feel that I have profitted from his enthusiastic character combined with the comfortable atmosphere for learning which he created.

I also want to thank all of my friends in the department for their suggestions and comments and for their friendship in general.

The final person I want to thank is KoKo Himes for the time she spent typing this thesis.

Some of the financial support for this work was provided by the National Science Foundation.

Chapter 1

INTRODUCTION

The desire to understand the unusual behavior associated with some of the properties of water has been the motivation behind various studies conducted in recent years. Some of the better known yet still peculiar properties associated with water are that it expands when it freezes, it has a density maximum at $4^{o}C$, and its viscosity is reduced when pressure is applied. These, along with other unique properties, have inspired scientists to take a closer look at one of our planet's most abundant resources.

Recent investigations have shown that additional peculiarities arise in supercooled water. In this region, anomalous behavior has been seen in a variety of thermodynamic[1,2] and transport properties.[3] Each of these divergent properties appears to have a singularity at $-45^{o}C$. This is evidence that a limit of stability and hence a second-order phase transition might exist at that temperature.

Researchers have found[4] that when some hydrophilic solutes are dissolved in water, the anomalies disappear. This is an indication that the water structure causing the anomalous behavior is being disrupted by the solute. However, others[5,6] have seen that when the mixed solute ethanol is dissolved in water, the anomalies in the viscosity and electric conductivity are enhanced. This suggests that the ethanol is promoting the formation of open polyhedral structures of hydrogen bonded water molecules which then create the enhancement. These structures are

known as clathrates.[7,8,9]

An improved understanding of the unusual properties of water clearly must lie in an improved understanding of the nature of its structure. A goal of this research has been to gain information about that structure and thus to further the effort to improve our understanding of it.

The research that shall be presented in this thesis consists of quasi-elastic light-scattering studies performed on aqueous solutions of the mixed solute tertiary-butyl alcohol at various concentrations. The selection of tertiary-butyl alcohol was made because its size and shape make it an effective clathrate former. An apparatus was constructed to hold the sample solution which was capable of controlling its temperature from above the boiling point to below the experimental limit of supercooling. The method used to study the light scattered from the liquid samples was photon correlation spectroscopy. With this method it was possible to determine the correlation time for each concentration from the Rayleigh component of the scattered light. This was done over a range of temperatures.

The experiment was divided into two parts. The first part was the measurement of correlation times for the pure solutions. These measurements were made at several temperatures for each concentration, including in the supercooled regime for some solutions. In the second part of the experiment, the viscosities of each solution were determined. This was done by two methods. For some concentrations flow measurements were used. For the other concentrations a light scattering technique was employed.

With the correlation time and the viscosity determined, the Stokes-Einstein diffusion equation was used to find a correlation length at various temperatures for each solution. These correlation lengths are related to the effective sizes of the clathrate structure forming. The

measurements made on the supercooled solutions provided a search for some indication of a singularity in the correlation length which could be related to the singularity in supercooled water.

Chapter 2

BACKGROUND SURVEY

It is reasonable to assume that some knowledge of the investigations which have been done on water and various aqueous solutions might generate a better understanding of the research contained within this thesis. Therefore, it seems appropriate at this point to present some of the ideas that have been provided by these investigations.

Among the various properties of water which have prompted study, of particular interest here are the thermodynamic properties of isobaric heat capacity and isothermal compressibility and the transport property, shear viscosity. Each has been shown to behave similar to a normal liquid at higher temperatures but to exhibit an anomalous increase with decreasing temperature into the supercooled region.

In 1976, Speedy and Angell[2] measured the isothermal compressibility (K_T) down to -26°C and saw an anomalous increase. They found that the behavior of K_T could be described by a power-law dependence in T, the temperature, with the existence of a singularity temperature T_S similar to the critical temperature found in critical phenomena. This power-law was of the form

$$X = X_o(T-T_S)^{-\gamma}$$

with γ representing a critical exponent. After applying this equation to some data supplied by other parties, they discovered that this description was not limited to K_T but could also be used for other properties, including the shear viscosity and the heat capacity. In each case it seemed

Figure 2-1 ANOMALOUS BEHAVIOR IN SUPERCOOLED WATER

Shown here as an example of an unusual property of water is the heat capacity.[10]

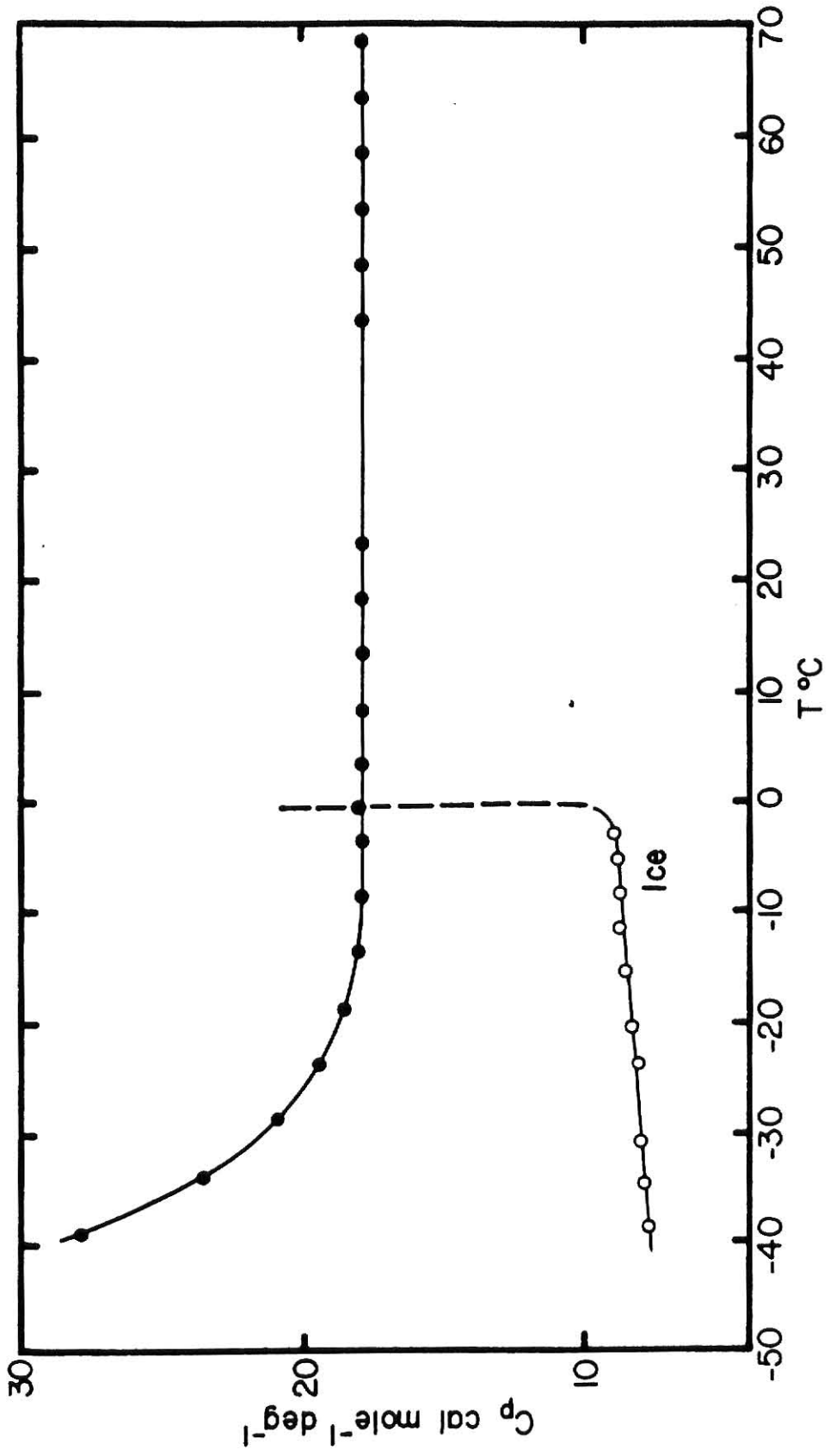
C_p cal mole^{-1} deg^{-1}
30
20
10
-50
-40
-30
-20
-10
0
10
20
30
40
50
60
70
T °C
Ice

that T_S = -45°C so that Speedy and Angell proposed the possible existence of a thermodynamic singularity at this temperature. This corresponded to a limit of mechanical metastability, meaning that the liquid was forced to make a transition of phase. The possible existence of a lambda-type transition had been predicted earlier. In another report,[11] Speedy discussed how the stability limits in superheated, stretched, supercooled, and normal water might all be linked together in some continuous fashion throughout the phase diagram.

The variations of these properties with temperature was believed to be associated with fluctuations in density and entropy. The nature of these fluctuations then became of interest. The idea that the fluctuations might be the result of some type of hydrogen bonded network seemed plausible since water was known to hydrogen bond with itself. The results of small angle x-ray scattering from H_2O, D_2O, and ethanol-water mixtures[12] showed an implication of increased density fluctuations with decreasing temperature. When the hydrogen bonding impurity ethanol was added, the correlation length (which had increased to about 8Å at -20°C) was reduced.

If indeed this hydrogen bonding was responsible for the fluctuations, then it was thought that the addition of hydrogen bonding impurities known to disrupt the association between the water molecules should also disrupt the fluctuations and therefore destroy the anomaly. Measurements of the specific heat and compressibility of aqueous solutions containing these impurities were made,[4] and indeed, the anomaly was disrupted as expected.

The anomaly was also affected by applying structure breaking pressure to the water.[13] This produced what seemed to be a shift in T_S. As the pressure was increased, the value of T_S decreased, following parallel to

the homogeneous nucleation temperature in the phase diagram.

In an effort to understand the structure produced by the bonding between water molecules and the relation of this structure to the properties of supercooled water, Stanley and Teixeira[14] developed a percolation model of water. Their model dealt with the connectivity of the water molecules through the hydrogen bonding. As the temperature decreased, the molecules became more connected. Although successful in qualitatively explaining the anomalies, it did not predict the singularity at $-45^{o}C$.

Another idea suggested by Stillinger[8] dealt with clathrate structures thought to form spontaneously in water. A clathrate is an open, cage-like polyhedron of hydrogen bonded water molecules. Solid clathrates are known to form under certain conditions in exact proportions between the solute and water and are static structures. When a mixed solute is added to water, the hydrophilic group keeps the solute in solution while the hydrophobic group promotes association between the water molecules. The combination of these two effects leads to the clustering of hydrogen bonded water molecules around the solute, thus forming a clathrate with a solute molecule filling the opening inside the structure. What Stillinger suggested was that perhaps the anomalous behavior was linked to the presence of liquid clathrates forming in pure water. Unlike the solid clathrates, these structures were thought to be continuously breaking and reforming and their concentration was believed to increase as the temperature decreased.

Halfpap and Sorensen[5] saw a diminishment of the anomaly in the viscosity when hydrazine was added to water similar to the effect others had seen on the specific heat.[4] However, contrary to their expectations at that

time, they found that the addition of ethanol created an enhancement of the anomalous behavior. Scientists had long been aware that aqueous solutions of mixed solutes such as ethanol exhibited unusual properties. It was thought that these properties might be a structural effect. Halfpap and Sorensen tied this together with Stillinger's idea to explain the enhanced anomaly they saw. Their explanation was that the addition of ethanol was inducing clathrate formation in the water and the increased concentration of clathrates caused an increase in the viscosity. They also proposed that since the addition of ethanol increased the clathrate concentration then an effective lower temperature was obtained in the water by adding the ethanol. To test this idea, they shifted the viscosity data in temperature for the ethanol-water solutions and found that over a substantially large temperature range the shifted data coincided well with the pure water data. The amount of the shift corresponded to the effective temperature drop.

Interest was thus generated in studying another good clathrate forming solute. The dissolution of such a solute into water is characterized by an overall loss of enthalpy due to the heat given off from the water-water hydrogen bonding and a loss of entropy as a result of the increased order of the system. The mixed solute tertiary-butyl alcohol (TBA), which contains a hydrophobic group in the form of $(CH_3)_3C$ and a hydrophilic OH, has been shown to produce an enthalpy loss when mixed with water at lower concentrations.[15] The TBA molecule is also comparable in size to the inner cavity of a clathrate and thus is an ideal solute to promote clathrate formation.

In view of the apparent nature of TBA to induce clathrates, various studies were done on TBA-water solutions. Small angle x-ray scattering

from TBA-water mixtures has shown a maximum tendency to form clusters in the range where $0.1 \leqslant X_{TBA} \leqslant 0.2$.[16] From these x-ray measurements, the size of the clusters in the $X_{TBA} = 0.11$ solution was estimated to be 20 Å. These results are coincidental with the value $X_{TBA} = 0.12$ where the ultrasonic absorption was found to be maximum.[17]

Several years later, Iwasaki and Fujiyama[18] measured the intensity of light scattered from TBA-water to see how the intensity varied with concentration. Interestingly, the maximum intensity seemed to be at $X_{TBA} = 0.13$. The intensity increased sharply in the $0 \ll X_{TBA} \leqslant 0.13$ region and then decreased less rapidly at higher concentrations. From their results they formed a model for the structure in different concentration regions.

The answer to why the anomalies exist in various properties of supercooled water probably lies in the water's structure. Based upon the evidence that was presented, the nature of this structure might be explainable with the use of a clathrate model. The characteristics of TBA along with the results of studies made on TBA-water[15] indicate that TBA is perhaps one of the best clathrate formers. Thus the basis of this thesis is to use photon correlation spectroscopy to investigate TBA-water solutions in an effort to gain a better understanding of clathrate formation and its relation to the behavior of supercooled water.

Chapter 3

PHOTON CORRELATION SPECTROSCOPY

When a plane electromagnetic wave is incident on a nonmagnetic, non-absorbing, nonconducting liquid medium, part of the field is scattered away from the incident direction. This scattering is a result of microscopic density fluctuations $\delta\rho(t)$ which produce corresponding fluctuations in the dielectric constant $\delta\varepsilon(t)$ and the index of refraction $\delta n(t)$. These then cause fluctuations in the scattered field which can provide information about the temporal behavior of the liquid. A useful method of acquiring this information is photon correlation spectroscopy (PCS). Below is given a concise description of PCS which has been derived from various sources.[19,20,21,22]

The incident electromagnetic wave mentioned above can be expressed in the form

$$\vec{E}_i(r,t) = \vec{E}_o \exp\, i(\vec{k}_o \cdot \vec{r} - \omega_o t) \qquad (3\text{-}1)$$

where E_o is the amplitude of the field, $\vec{k}_o$ represents the propogation vector, and ω_o is the angular frequency. The amount of the field which is scattered is dependent upon the magnitude as well as the spatial size of the fluctuations. Also, as will be shown, the spectrum of the field is dependent upon how $\delta\rho(t)$ varies in time.

Now if $\vec{k}_f$ is the propogation vector for the field scattered at an angle θ in the direction of some detector (see Fig. 3-1), then a scattering vector $\vec{q}$ can be defined by the incident and scattered propogation vectors as

Figure 3-1 SCATTERING GEOMETRY AND THE SCATTERING VECTOR

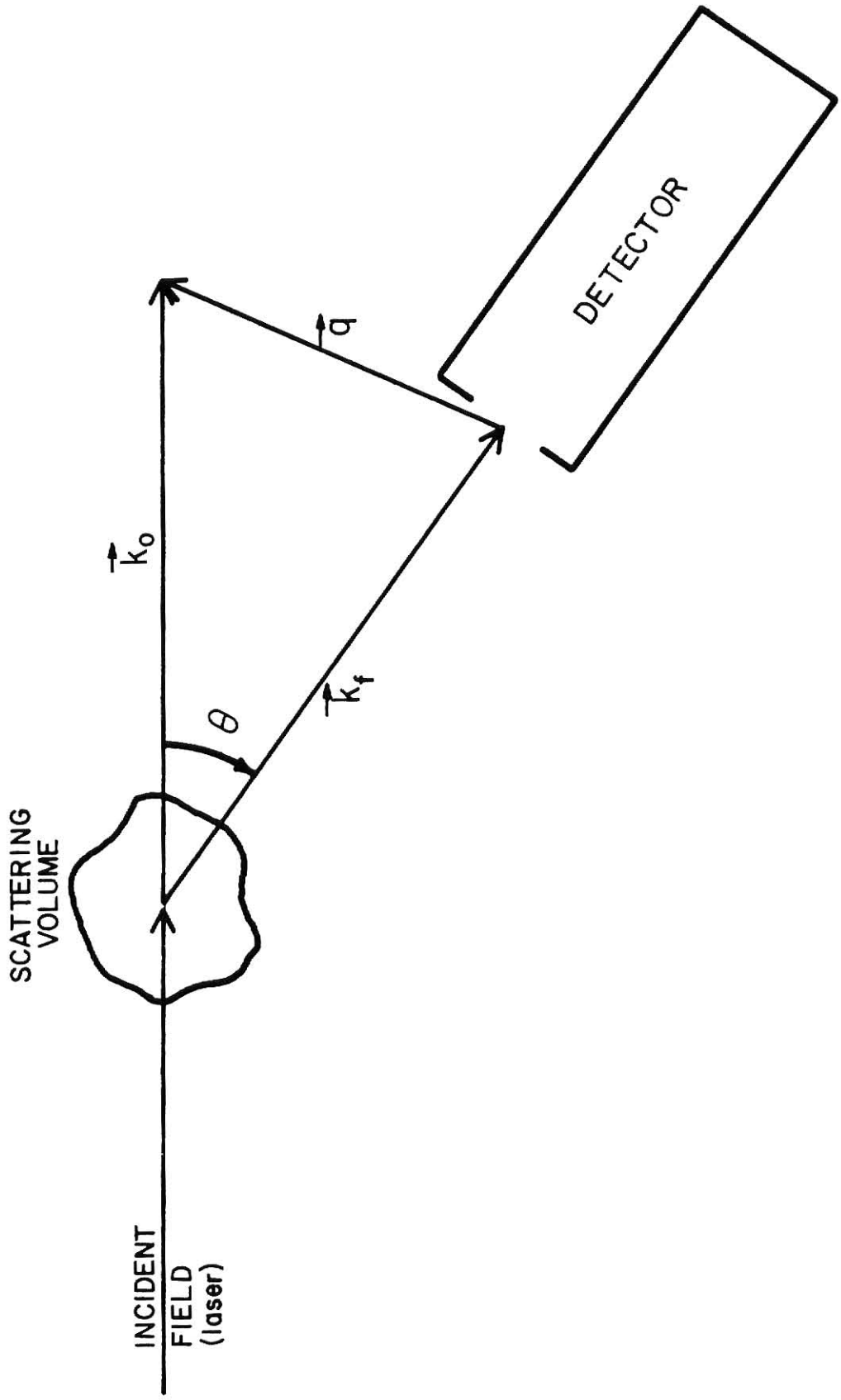
DETECTOR
$\vec{q}$
$\vec{k}_o$
$\vec{k}_f$
θ
SCATTERING VOLUME
INCIDENT FIELD (laser)

$$\vec{q} = \vec{k}_o - \vec{k}_f. \tag{3-2}$$

If the scattering is quasi-elastic, then $k_o \cong k_f$ and it can easily be shown that

$$q = 2k_o \sin \frac{\theta}{2} . \tag{3-3}$$

By definition the magnitude of the propogation vector is

$$k_o = \frac{2\pi n}{\lambda_o} \tag{3-4}$$

where λ_o is the wavelength of the incident field in vacuum and n is the index of refraction of the liquid, thus

$$q = \frac{4\pi n}{\lambda_o} \sin \frac{\theta}{2} . \tag{3-5}$$

Let $E_s(R,t)$ designate the scattered field at the detector which is at a distance R from the scattering volume. The vector notation can be omitted because the polarization of the field does not change with time. Since fluctuations in the dielectric constant $\delta\varepsilon(t)$ arise from $\delta\rho(t)$, $E_s(R,t)$ can be linked to $\delta\rho(t)$. In other words, the spectrum of $E_s(R,t)$ is produced by $\delta\rho(t)$ and thus from looking at that spectrum the time variation of $\delta\rho(t)$ can be described. This is done with the use of an autocorrelation function of the scattered field. Therefore, a description of the autocorrelation function follows.

Consider some property A(t) which behaves like a randomly varying noise signal as illustrated in Fig. (3-2). The time autocorrelation function of A(t) is defined as the time average

$$\langle A(t)A(t+\tau)\rangle = \lim_{T\to\infty} \frac{1}{T} \int_{t_o}^{t_o+T} dt\, A(t)A(t+\tau). \tag{3-6}$$

For a stationary property this correlation function is independent of the initial time and thus can be written as

$$\langle A(0)A(\tau)\rangle = \lim_{T\to\infty} \frac{1}{T} \int_{0}^{T} dT\, A(t)A(t+\tau). \tag{3-7}$$

Figure 3-2 DETECTED SIGNAL AND THE BEHAVIOR OF AN AUTOCORRELATION FUNCTION

The first figure[19] shows typically the nature of the signal detected at the photomultiplier. The second figure[19] illustrates the exponential decay exhibited by an autocorrelation function.

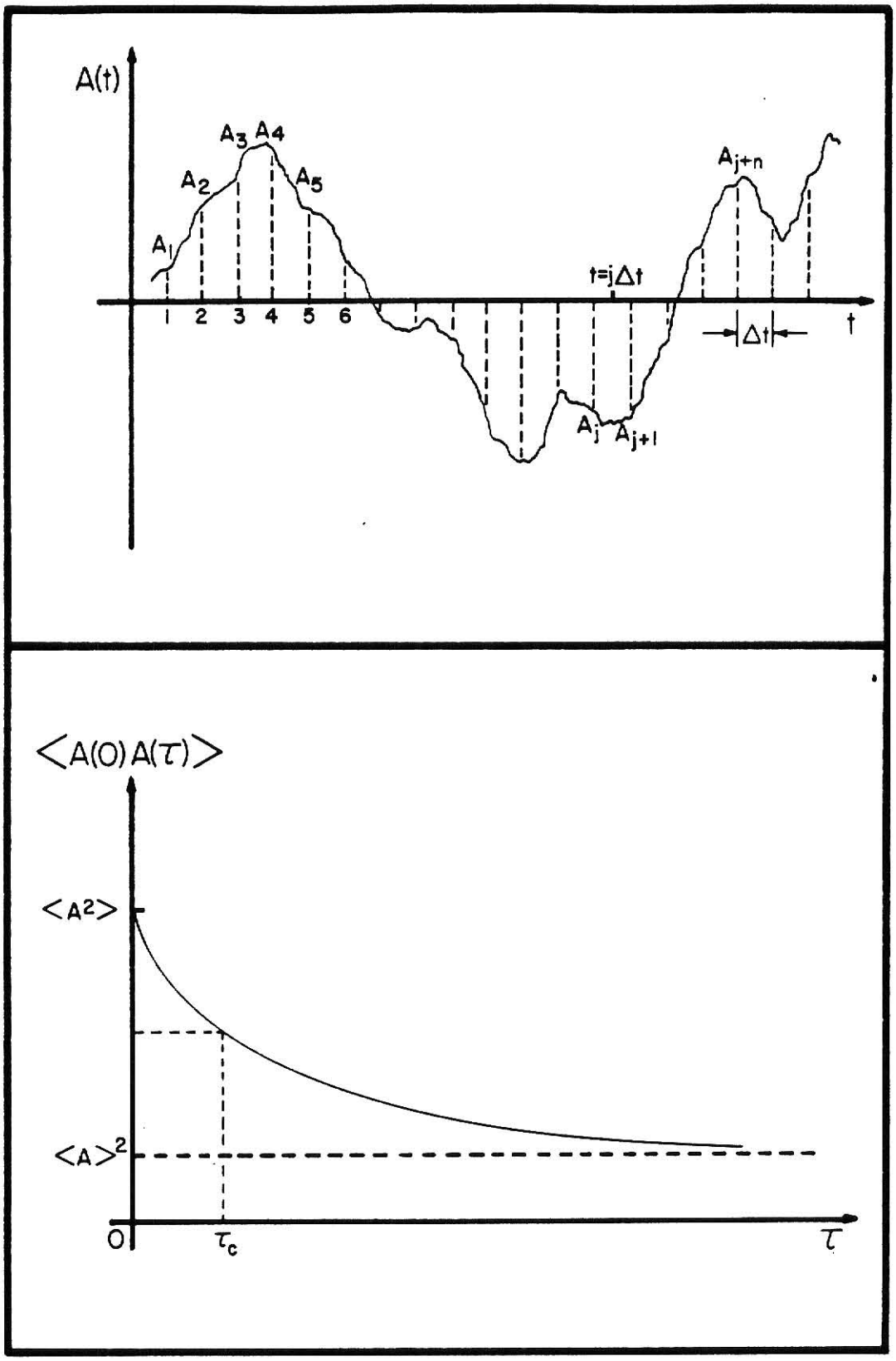
A(t)
A1
A2
A3
A4
A5
Aj+n
t=jΔt
1
2
3
4
5
6
Δt
t
Aj
Aj+1
<A(0)A(τ)>
<A2>
<A>2
0
τc
τ

Notice that the time scale in Fig. (3-2) has been divided into intervals of length Δt. This digitizes $A(t)$ so that A_j denotes the average value of $A(t)$ over the interval $t = j\Delta t$ to $t = (j+1)\Delta t$ and likewise A_{j+m} denotes the average value of $A(t)$ over the interval $t = (j+m)\Delta t$ to $t = (j+m+1)\Delta t$. Under this procedure the correlation function can be approximated by changing the integral to a summation,

$$\langle A(0)A(\tau)\rangle \cong \lim_{N\to\infty} \frac{1}{N} \sum_{j=1}^{N} A_j A_{j+m}, \tag{3-8}$$

where $\tau = m\Delta t$.

When $\tau = 0$,

$$\langle A(0)A(\tau)\rangle = \langle A(0)^2\rangle \tag{3-9}$$

and all of the terms in the summation are positive. As τ increases, some of the terms become negative as can be seen in Fig. (3-2) so that some of the terms in the summation of Eq. (3-8) are negative. This leads to the condition

$$\langle A(0)^2\rangle \geqslant \langle A(0)A(\tau)\rangle. \tag{3-10}$$

For large values of τ, $A(0)$ becomes uncorrelated with $A(\tau)$ so that

$$\lim_{T\to\infty} \langle A(0)A(\tau)\rangle = \langle A(0)\rangle\langle A(\tau)\rangle = \langle A\rangle^2. \tag{3-11}$$

The correlation function then must decay from its maximum value at $\langle A^2\rangle$ to its lower limit at $\langle A\rangle^2$. In many cases this decay is exponential with its behavior described by

$$\langle A(0)A(\tau)\rangle = \langle A\rangle^2 + [\langle A^2\rangle - \langle A\rangle^2] \exp(-\frac{\tau}{\tau_c}) \tag{3-12}$$

where τ_c is the correlation or relaxation time of the function (see Fig. 3-3).

It is interesting to note that by virtue of the Wiener-Khintchine theorem the time correlation function and the spectral density are Fourier transforms of each other,

$$I(\omega) = \frac{1}{2\pi}\int_{-\infty}^{\infty} d\tau\ G(\tau)\exp(-i\omega t) \tag{3-13}$$

$$G(\tau) = \int_{-\infty}^{\infty} d\omega\ I(\omega)\exp(i\omega t). \tag{3-14}$$

$I(\omega)$ has been used to represent the spectral density and $G(\tau)$ is the correlation function. The same information can be gained from either the correlation function or the spectral density. However, the data supporting this thesis was obtained from measurements of a correlation function rather than a spectral density.

Now that the time autocorrelation function for some general property $A(t)$ is established, replace $A(t)$ with the scattered field at the detector. The autocorrelation function for $E_s(R,t)$ is then

$$\begin{aligned} \langle E_s^*(R,0)E_s(R,\tau)\rangle &= \lim_{T\to\infty}\frac{1}{T}\int_0^T dt\ E_s^*(R,t)\ E_s(R,t+\tau) \\ &\cong \lim_{N\to\infty}\frac{1}{N}\sum_{j=1}^{N} E_{sj}^* E_{sj+m}. \end{aligned} \tag{3-15}$$

However, when a square law detector, such as a photomultiplier tube, is used, the electric field can't be detected. Instead the intensity which is proportional to the number of photons entering the detector is measured. The property of interest then is the number of photons entering the detector at time t which is denoted by $n(t)$. The autocorrelation function for $n(t)$ is

$$\langle n(0)n(\tau)\rangle = \lim_{T\to\infty}\frac{1}{T}\int_0^T dt\ n(t)n(t+\tau) \cong \lim_{N\to\infty}\frac{1}{N}\sum_{j=1}^{N} n_j n_{j+m}. \tag{3-16}$$

This can be linked back to $E_s(R,t)$ by first noting the relationship between the autocorrelation function of $n(t)$ and of the intensity, $I(t)$,

$$\langle n(0)n(\tau)\rangle = (aT)^2\langle I(0)I(\tau)\rangle \tag{3-17}$$

Here a is the quantum efficiency of the detector while T is known as the sample time, equivalent to Δt discussed earlier. The intensity is in turn

related to the scattered field at the detector by

$$I = \alpha|E_s(R,t)|^2 \tag{3-18}$$

with α representing a proportionality constant.

Experimentally, two different optical mixing techniques can be used in obtaining the autocorrelation function of the scattered field. One technique is the homodyne or self-beating method in which only the scattered field enters the detector. The other technique is the heterodyne method. Here a local oscillator is mixed with the scattered field on the detector.

First consider a situation in which homodyne detection is applied. If, as in a liquid, the number of independent scattering regions is large, then a Gaussian approximation can be used to express the autocorrelation function of the intensity in terms of the scattered field,

$$\langle I(0)I(\tau)\rangle = \alpha^2\langle|E_s|^2\rangle^2 + \alpha^2|\langle E_s^*(0)E_s(\tau)\rangle|^2. \tag{3-19}$$

The second term on the right, as will be shown later, decays exponentially in time,

$$\langle E_s^*(0)E_s(\tau)\rangle = \langle|E_s|^2\rangle \exp(-\Gamma\tau - i\omega_0\tau), \tag{3-20}$$

so that

$$\langle I(0)I(\tau)\rangle = \alpha^2\langle|E_s|^2\rangle^2[1+\exp(-2\Gamma\tau)] = \langle I\rangle^2 [1+\exp(-2\Gamma\tau)]. \tag{3-21}$$

The intensity fluctuations have Lorentzian spectral density with half-width $\Gamma = \frac{1}{\tau_c}$. It follows directly from Eq. (3-17) that

$$\langle n(0)n(\tau)\rangle = (aT)^2\langle I\rangle^2[1+\exp(-2\Gamma\tau)]. \tag{3-22}$$

In a similar fashion, for heterodyne detection it can be shown that

$$\langle I(0)I(\tau)\rangle \cong \beta I_{LO}^2 + 2\beta I_{LO}\mathrm{Re}\,\langle E_s^*(0)E_s(\tau)\rangle \tag{3-23}$$

where I_{LO} is the intensity of the local oscillator at the detector and β is a constant. By again making use of Eq. (3-20), this becomes

$$\langle I(0)I(\tau)\rangle \cong \beta I_{LO}[I_{LO} + 2\langle I\rangle \exp(-\Gamma\tau)\cos(\omega_{LO}-\omega_o)\tau] \tag{3-24}$$

and the photon count autocorrelation function is

$$\langle n(0)n(\tau)\rangle \cong (aT)^2\beta I_{LO}[I_{LO} + 2\langle I\rangle \exp(-\Gamma\tau)\cos(\omega_{LO}-\omega_o)\tau]. \tag{3-25a}$$

Notice that in the heterodyne method, ω_o is replaced with the difference between the local oscillator frequency ω_{LO} and the frequency of the incident field. When $\omega_{LO} = \omega_o$, Eq. (3-25a) becomes

$$\langle n(0)n(\tau)\rangle = (aT)^2\beta I_{LO}[I_{LO} + 2\langle I\rangle \exp(-\Gamma\tau)\tau]. \tag{3-25b}$$

The details leading to this expression might be difficult to discern from standard treatments such as that presented by Berne and Pecora.[19] That is why a somewhat explicit approach has been used here.

The random fluctuations in the liquid are not static but instead are constantly forming and decaying away. The behavior of the fluctuation is produced by diffusion processes in the liquid described by the equations

$$\frac{\partial \rho}{\partial t} = -D_m \nabla^2 \rho \tag{3-26}$$

for mass or concentration diffusion and by

$$\frac{\partial T}{\partial t} = -D_T \nabla^2 T \tag{3-27}$$

for thermal diffusion where D_m and D_T are the mass and thermal diffusion constants respectfully (a more thorough description of D_m and D_T will be presented later). It becomes apparent that the behavior of $\delta\varepsilon(t)$ is governed by a diffusion equation of the form seen in Eqs. (3-26) and (3-27).

To illustrate how the nature of the diffusion is deduced, Clark

Lunacek, and Benedek show that for a system of particles undergoing Brownian motion, the autocorrelation function of the scattered field can be written as

$$\langle E_s^*(t)E_s(t+\tau)\rangle = E_s'^2\exp(-i\omega_o\tau)\ \langle \sum_k \sum_j \exp\{-i[\phi_k(t)-\phi_j(t+\tau)]\}\rangle \tag{3-28}$$

where E_s' represents the amplitude of the scattered field from each particle and $\phi_k(t)$ is a phase factor given by

$$\phi_k(t) = \vec{q}\cdot\vec{r}_j(t). \tag{3-29}$$

Each summation is over all particles in the scattering volume. After the ensemble average is taken, only k=j terms remain because different particles diffuse randomly. Thus if N is the number of particles involved,

$$\langle E_s^*(t)E_s(t+\tau)\rangle = NE_s'^2\exp(-i\omega_o\tau)\langle\exp[-i\vec{q}\cdot\vec{r}(t)-\vec{r}(t+\ )]\rangle. \tag{3-30}$$

The ensemble average is the average of the phase term weighted with the probability distribution for the particle diffusion

$$\langle\exp(-i\vec{q}\cdot\Delta\vec{r})\rangle = \int_{-\infty}^{\infty} d^3\Delta\vec{r}\ P(\Delta\vec{r},\tau|0,0)\exp(i\vec{q}\cdot\Delta\vec{r}) \tag{3-31}$$

where $P(\Delta\vec{r},\tau|0,0)\ d^3\Delta\vec{r}$, the probability that a particle at a point (0,0) will be located in a volume of size $d^3\Delta r$ around a point defined by the position vector Δr after a time τ, is the solution to the diffusion equation given by

$$P(\Delta\vec{r},\ t|0,0)d^3\Delta r = (4\pi Dt)^{-\frac{3}{2}}\exp(-\frac{\Delta r^2}{4Dt}). \tag{3-32}$$

The correlation function then becomes

$$\langle E_s^*(t)E_s(t+\tau)\rangle = NE_s'^2\exp(-Dq^2\tau-i\omega_o t). \tag{3-33}$$

Although Eq. (3-33) is derived for particle diffusion, the solution is general and applies for thermal and concentration diffusion as well.

By comparing Eq. (3-33) to Eq. (3-20), it becomes apparent that

$$\Gamma = \frac{1}{\tau_c} = Dq^2. \tag{3-34}$$

The form of the constant D depends on the type of diffusion. For mass or particle diffusion the Stokes-Einstein equation applies,

$$D_m = \frac{k_B T}{6\pi\eta r} \tag{3-35}$$

where k_B is Boltzman's constant, T is the temperature, η is the viscosity, and r is the radius of the particles which are diffusing. For thermal diffusion the diffusion constant is given by

$$D_T = \frac{\Lambda}{\rho_o C_P} . \tag{3-36}$$

Here ρ_o is the average density, C_P represents the isobaric heat capacity, and Λ is the thermal conductivity. Replacing the radius with the correlation length ξ in Eq. (3-35) will yield the diffusion constant for concentration diffusion. The correlation length can be described as the minimum separation between two particles moving independent of each other. In other words, if two particles are less than a distance ξ apart, then the motion of one is not independent of the motion of the other.

Notice that Eqs. (3-34) and (3-35) can be used to obtain an expression relating the correlation time to the viscosity. Therefore if the size of the particle undergoing diffusion is known, the viscosity can be determined by measuring τ_c. Likewise, if the viscosity is known the size of the particles (or perhaps the correlation length) is obtainable from τ_c.

In practice, the correlation function measured is not in general a true exponential. Under experimental conditions the function can be fit to an equation of the form

$$B + A \exp(-K_1 t + \frac{K_2}{2} t^2). \tag{3-37}$$

In this expression, B is due to a measure of the background contribution resulting from a lack of coherence on the photomultiplier, dark counts in the detector, extraneous light, vibrations, etc., A is the signal amplitude, and K_2 is a fitting parameter which provides an indication of how well the function compares to a true exponential. Ideally the second term in the exponential should be very small in relation to the first term,

$$(K_1 t)^2 >> \frac{K_2}{2} t^2.$$

Finally, K_1 determines the correlation time. For homodyne detection

$$K_1 = \frac{2}{\tau_c} \tag{3-38}$$

and for heterodyne detection

$$K_1 = \frac{1}{\tau_c} \, . \tag{3-39}$$

Chapter 4

EXPERIMENT

An argon ion laser operating at at wavelength of 514.5 nm served as a light source for the experiment. A lens of focal length 36.4 cm was used to focus the beam into a glass spectrophotometer cell whose dimensions were approximately 1 cm x 1 cm x 5 cm. The light scattered by the liquid sample contained within the cell was observed at one of two angles, either 25.8^{o} or 90^{o} (see Figure 4-1). A lens of focal length 12.0 cm located 25 cm from the scattering volume gathered the light and focused an image on an adjustable slit, 22 cm from the lens. The slit then defined the exact scattering volume which would be detected by a FW 130 photomultiplier and also determined how much of the light scattered by the cell walls would be detected. The scattered light then passed through an iris diaphram, down a 40 cm tube, and was detected at the cathode and photomultiplier. A movable mirror located in front of the cathode was used to view the scattering visually with the aid of a short working distance telescope.

The 25.8^{o} scattering angle was used to make measurements above the ambient temperature. As the scattering angle θ decreased, the apparent separation between the bright spots produced by the beam as it entered and exited the cell became less. On the other hand, as the angle increased the correlation time, which is being measured, decreased due to the $\sin^2 \frac{\theta}{2}$ dependence seen in Eqs. (3-3) and (3-34). The 25.8^{o} angle seemed to be large enough to overcome the problem of the bright spot separation and

Figure 4-1 SMALL ANGLE SCATTERING SETUP

(From M.S. thesis by B. L. Halfpap)

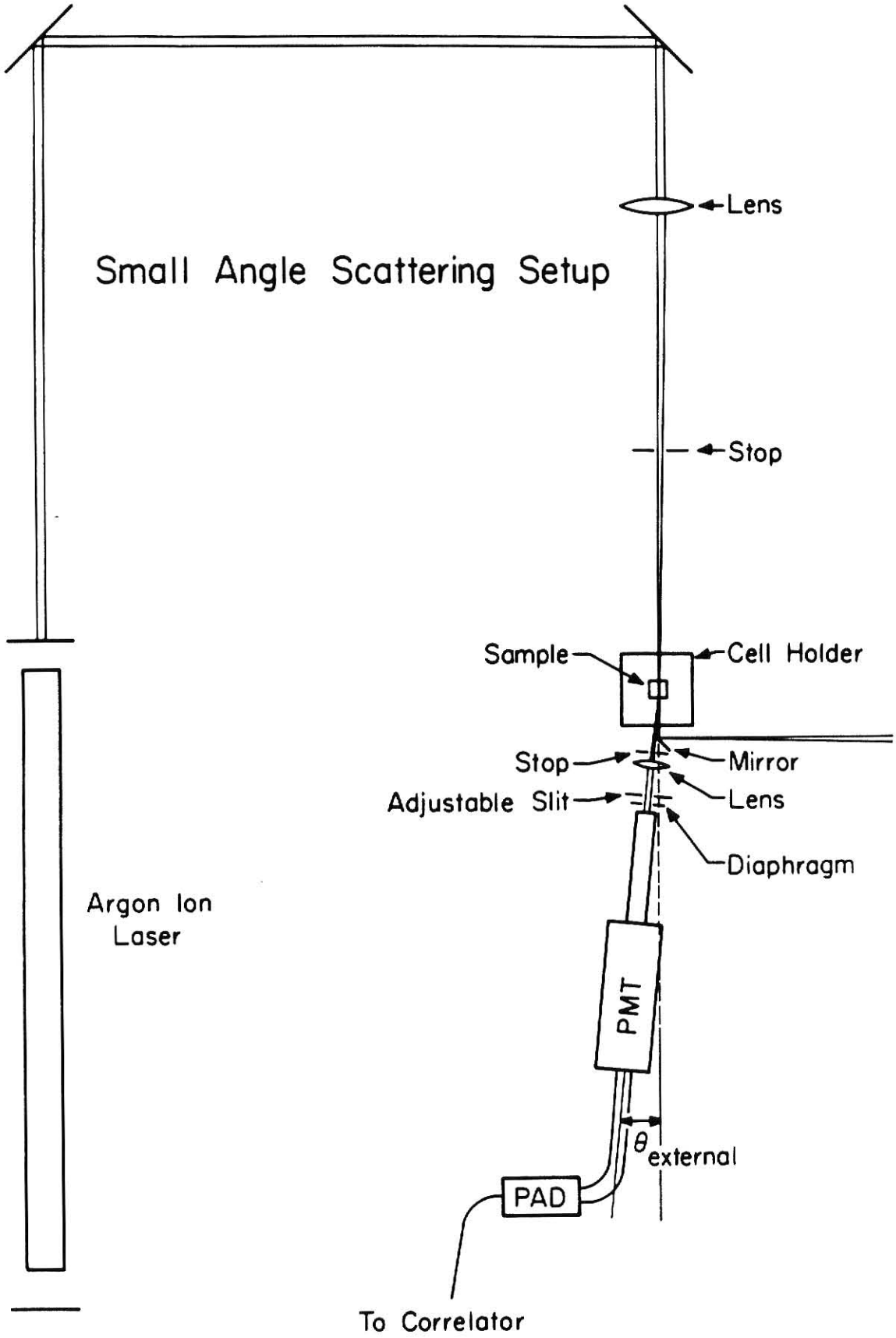
Small Angle Scattering Setup
Lens
Stop
Sample
Cell Holder
Stop
Mirror
Adjustable Slit
Lens
Diaphragm
Argon Ion Laser
PMT
θ external
PAD
To Correlator

still small enough to yield correlation times large enough to be measured with our correlator. Typical correlation times were $\tau_c \gtrsim 50$ μsec while our correlator is effective for $\tau_c \gtrsim 5$ μsec.

Below the ambient temperature the 90^o scattering angle was used. This geometry proved to be the simplest to employ mainly because the bright entrance and exit spots were at their largest separation allowing complete removal from detection. This then made it possible to produce a homodyne signal with high signal/background. The end result was less time required to collect data. As later will be seen, the correlation time became longer as the temperature decreased, thus permitting this larger angle to be used. At substantially long values, $\tau_c \gtrsim 10$ msec, the correlation time became very difficult if not impossible to measure due to an increased influence of external vibrations. However, by the same $\sin^2 \frac{\theta}{2}$ dependence mentioned in the previous paragraph, the correlation time was made shorter at 90^o and thus lower temperatures could be studied.

Two types of cells were used to contain the samples. One was constructed of glass and the other was quartz. The quartz cell was used for all smaller angle work because the superior finish of its surfaces produced less extraneous light from the bright spots when the beam passed through the cell walls. At 90^o, the large separation of these spots made this concern less critical and thus allowed use of the glass cell which in most cases, proved to be strong enough to withstand the expansion of the sample upon nucleation. This quality was seen not to be shared by the quartz version when one was broken by a sample that had nucleated.

The cells were held in place by a copper and brass assembly shown in Figure 4-2. The outer sleeve of this assembly was coated with red GLPT insulating varnish and then wrapped with heating coils.

Figure 4-2 CELL HOLDER

The spectrometer cells sits inside piece A and is held in place by B. This then slides into piece C and E fits around the entire assembly. Both C and E are wrapped with heating coils.

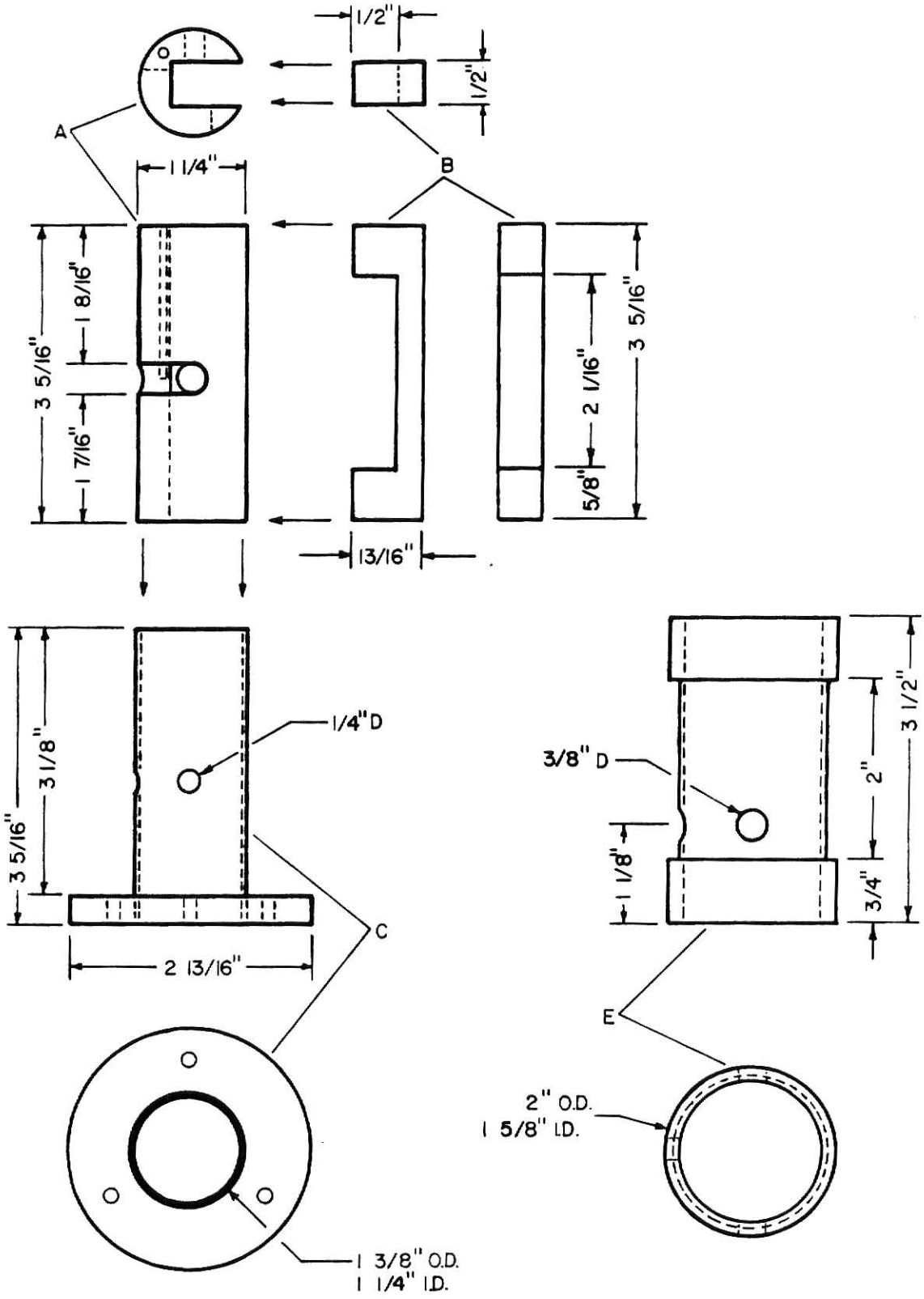
1/2"
1/2"
A
B
1 1/4"
3 5/16"
1 8/16"
1 7/16"
2 1/16"
5/8"
3 5/16"
13/16"
1/4" D
3 1/8"
3 5/16"
2 13/16"
C
3/8" D
1 1/8"
2"
3/4"
3 1/2"
E
2" O.D.
1 5/8" I.D.
1 3/8" O.D.
1 1/4" I.D.

Control of the temperature was accomplished by two different apparatuses. For temperatures above ambient, an aluminum sleeve wrapped with heating coils was constructed to fit loosely around the outside of the holder (Fig. 4-2). The coils were then attached to a variable AC voltage supply. The entire assembly was surrounded by a plexiglass tube and capped with styrofoam. The temperature was then controlled by selecting a setting on the voltage supply that was known to produce a temperature somewhere in the range of interest. The cell was allowed to come to equilibrium, using no active feedback. This temperature was stable to within $\pm 0.2^{o}C$ and was monitored by a YSI 44004 thermistor embedded in the holder near the cell itself. The thermistor was tied into a wheatstone bridge with an amplifier (hereafter referred to as a DC bridge) to measure the thermistor resistance and hence the temperature.

For temperatures below ambient a slightly more involved method was employed. Here a chamber was placed around the holder and this was insulated with polyethylene and styrofoam. Tubes were inserted into the chamber through the polyethylene and glass windows were attached to these tubes. The tubes extended approximately 8 cm outside of the polyethylene, thus allowing the glass windows to stay sufficiently warm to prevent frosting. Cold nitrogen gas was pumped into the chamber at a controlled rate. This was accomplished by flowing warm nitrogen gas through a flow meter into a dewar of liquid nitrogen. The nitrogen which then boiled off was forced out another tube into the chamber containing the cell holder. Once the temperature was at the level desired, the DC bridge was set to that temperature. Current was then supplied to the coils around the holder by a differential amplifier/power supply which was being automatically controlled by the DC bridge/thermistor arrangement.

Figure 4-3 COOLING CHAMBER ASSEMBLY

The cell holder is placed inside of the cylindrical canister E in the figure. The collar C then fits around the canister and the tube B slides into the hole on the side of C (likewise in the other two holes). The window A then slides over B. Styrofoam covers the remaining exposed portion of E.

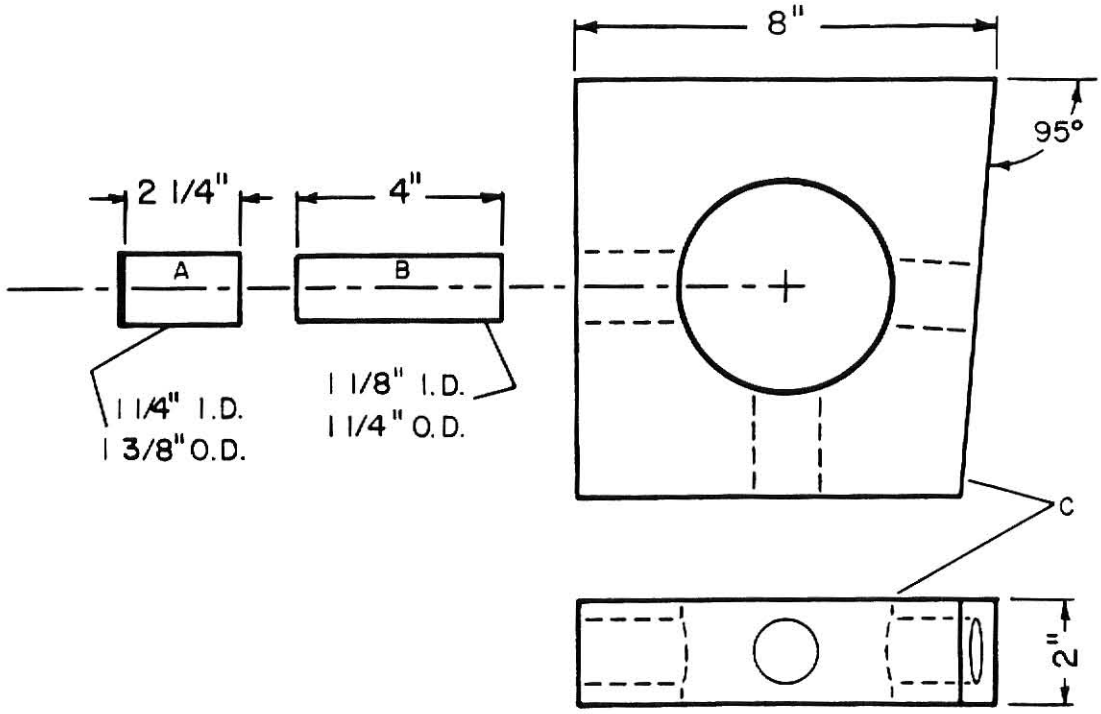
8"
95°
2 1/4"
4"
A
B
1 1/4" I.D.
1 3/8" O.D.
1 1/8" I.D.
1 1/4" O.D.
C
2"

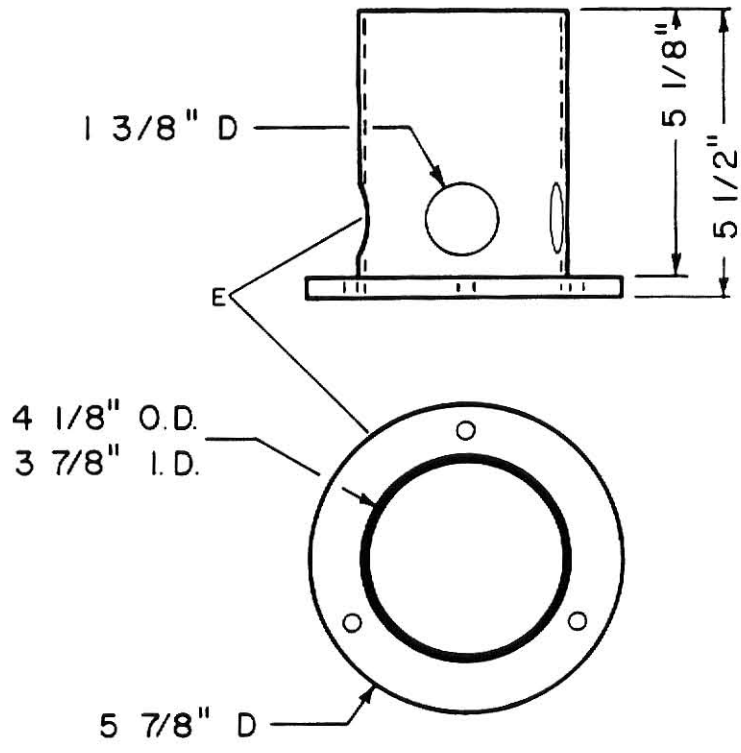
1 3/8" D
5 1/8"
5 1/2"
E
4 1/8" O.D.
3 7/8" I.D.
5 7/8" D

Figure 4-4 TEMPERATURE CONTROL ABOVE AMBIENT

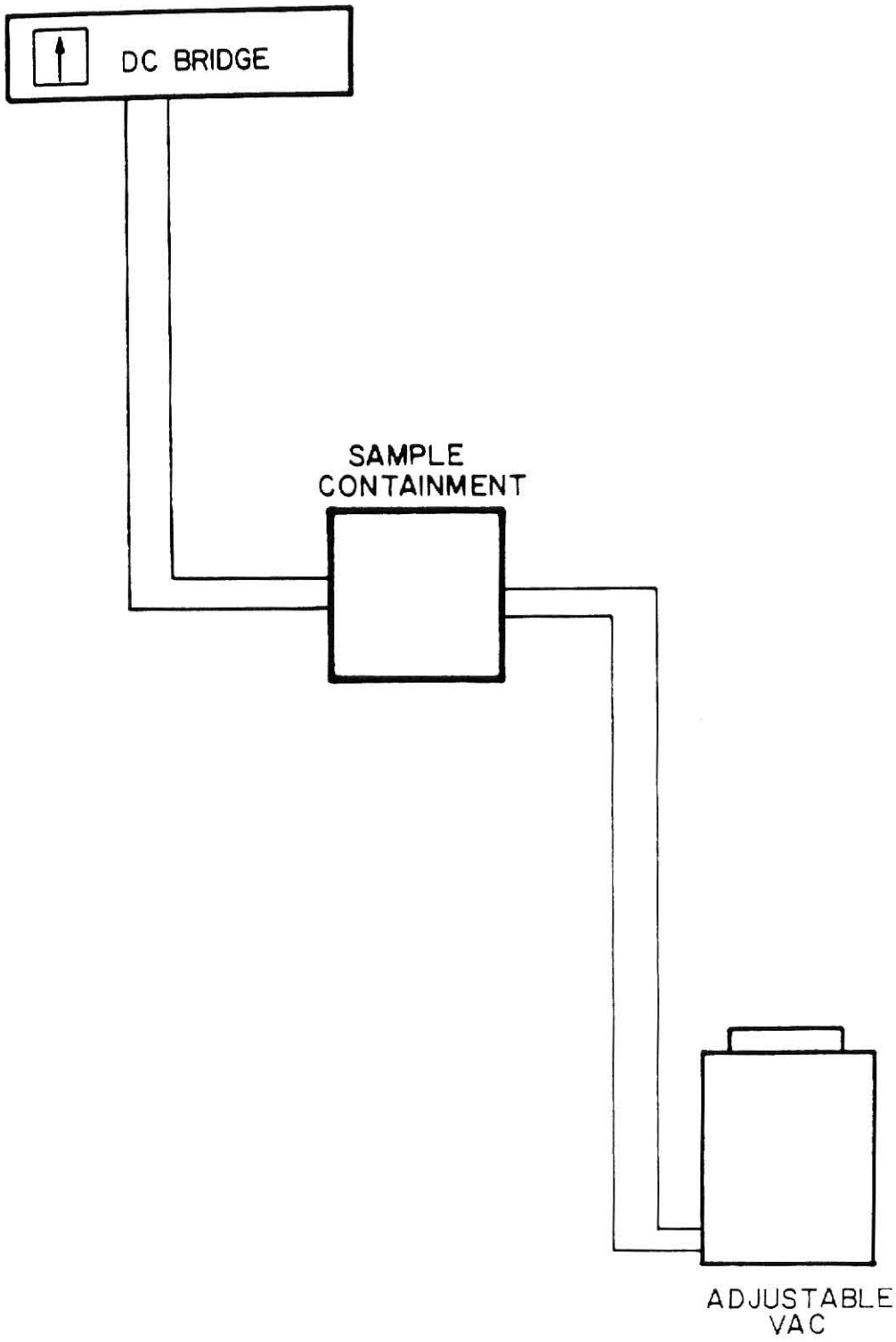
DC BRIDGE
SAMPLE
CONTAINMENT
ADJUSTABLE
VAC

Figure 4-5 TEMPERATURE CONTROL BELOW AMBIENT

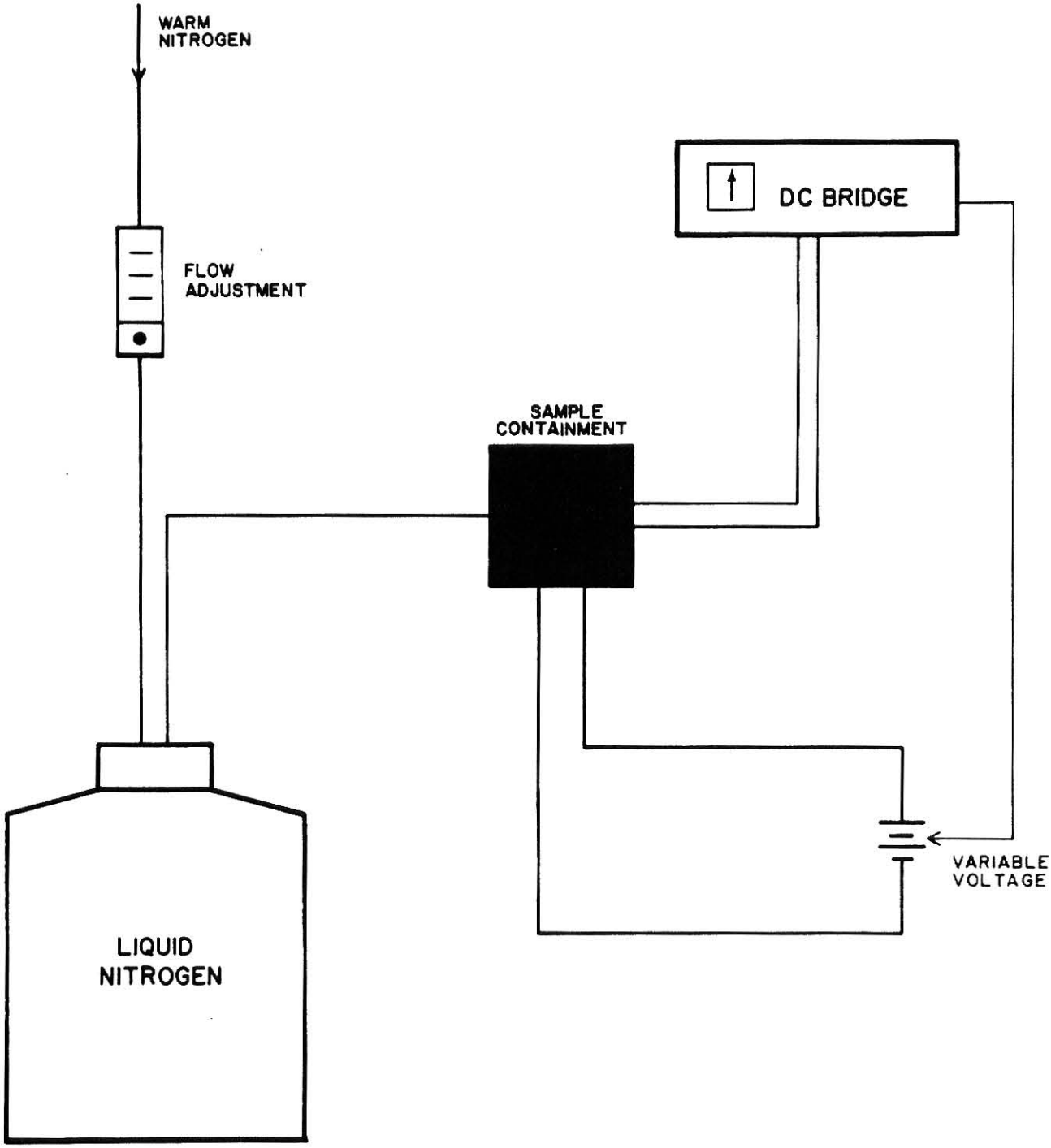
WARM
NITROGEN
DC BRIDGE
FLOW
ADJUSTMENT
SAMPLE
CONTAINMENT
VARIABLE
VOLTAGE
LIQUID
NITROGEN

Once again the cell was allowed to come to equilibrium. The stability of the temperature in this case was $\pm 0.1^{o}C$.

Preparation for the experiment began with a thorough cleansing of the sample cell. The first step to this procedure was to flush the inside and outside walls with warm, mild soap solution (Joy). Next the cell was placed (still emersed in the same soap solution) in an ultrasonic cleaner for approximately 10-15 minutes. Again the cell walls were flushed with the soap solution and then rinsed, first with tap water and then with distilled water. A final rinsing was performed with spec. grade acetone.

The sample itself was mixed in bulk to form stock solutions. A 0.2 μm Nucleopore filter was used to remove particulates. This filter was attached to a syringe which was first used to flush the inside of the cell with filtered solution and then to filter and load the solution in the cell.

A final step was taken prior to loading the cell into the holder. The outside walls of the cell were wiped with spec. grade acetone and lens paper. This was done to reduce the amount of light that would be scattered from a dirty surface. This step was of more concern during the 25.8^{o} scattering because in this arrangement the bright spots produced by the light beam at the cell walls become visually closer together. Thus if these spots become too bright, a significant amount of light scattered from the liquid would be washed out by the spots. As a result the desired signal would not be detected.

It should be noted that many times, any or all of the cleaning and filtering procedures had to be repeated. Failure to sufficiently perform these steps led to the presence of a significant number of foreign par-

Figure 4-6 SPECTROMETER CELL WALL SPOTS

(From M. S. thesis by B. L. Halfpap)

Spectrometer Cell Wall Spots

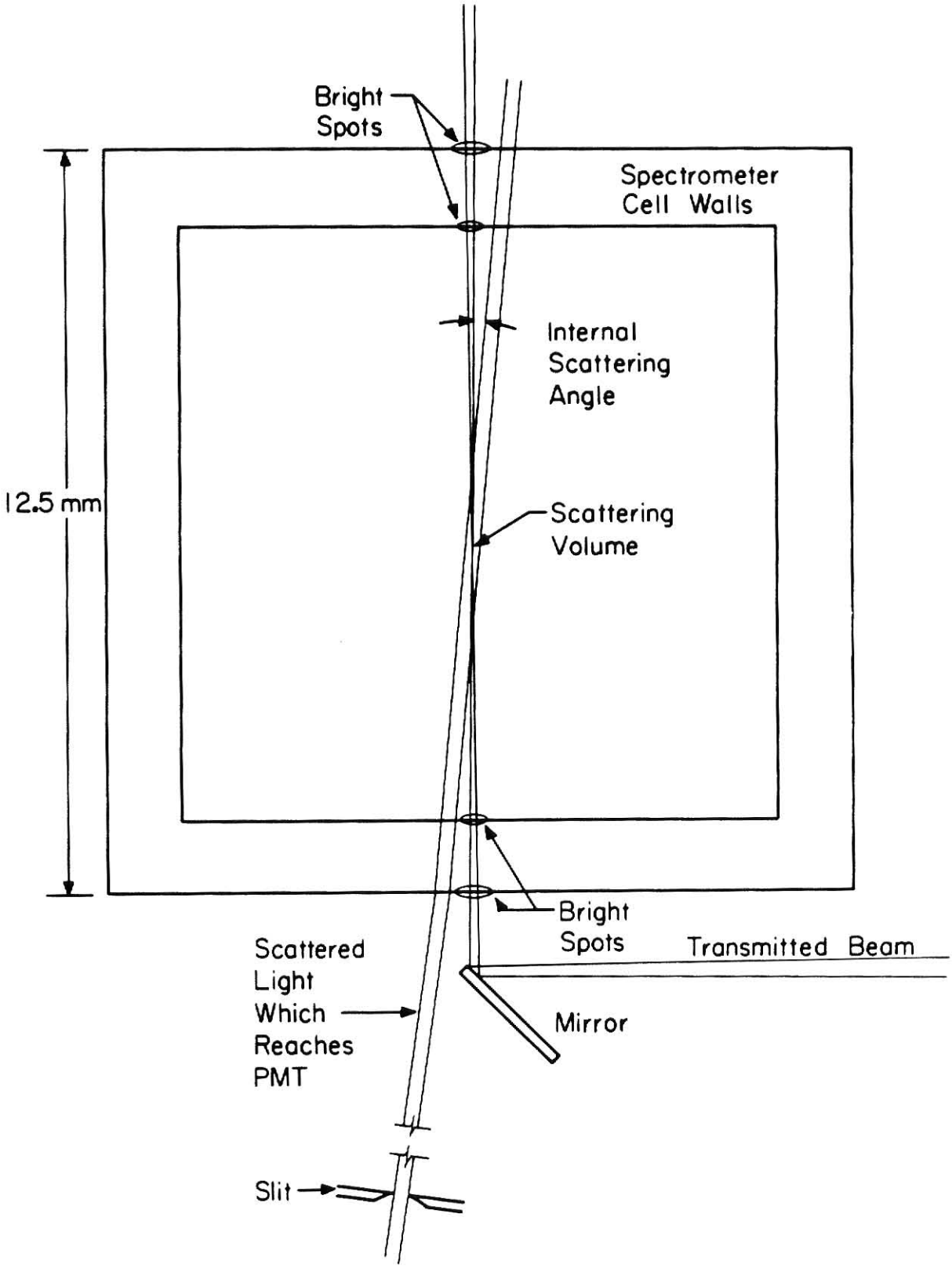

ticles in the sample which would form moats floating through the beam, scattering large amounts of unwanted light. On occasions, if the number of these moats was small, the sample was allowed to sit for several hours up to a day and the moats would settle out.

Once a satisfactory sample was obtained and the cell was loaded in the holder, the angles of the cell were adjusted so that the reflected beam (from cell walls) was aligned with the incident beam to insure that the beam was passing through square to the cell.

After the photomultiplier was at the desired angle, the slit had to be adjusted to select the scattering volume to be used. A heterodyne signal was used at 25.8^{o}, requiring that the slit was adjusted to allow a part of the wall spot to enter the photomultiplier. The wall spot acted as a local oscillator source and mixed with the signal from the liquid. On the other hand, a homodyne signal was used at 90^{o}. In this case, the slit was adjusted to sample a segment of the light scattered by the liquid somewhere near the center of the cell while omitting any part of the wall spots.

The photomultiplier detected the scattered light and this signal was passed through a pulse amplifier/discriminator (PAD). Here the signal was converted to 5V, 30 nanosecond square pulses (consistent with TTL logic). This converted signal was then sent to a Langley-Ford digital correlator. The resulting correlation function was relayed to a Digital PDP 11/34 computer where it was analyzed by a two cumulant least-square fit to the expected exponential form. Typical time required to obtain a single correlation function varied considerably (anywhere from around 5 to 90 minutes) and was dependent upon the correlation time as well as the quality of the signal.

By using Eqs. (3-34) and (3-35), the following expression could be derived

$$\frac{1}{q^2\tau_c} = \frac{k_B T}{6\pi\eta\xi} . \qquad (4\text{-}1)$$

So to acquire the correlation length ξ from a measurement of τ_c it was necessary to know the value of η, the viscosity.

In order to obtain the viscosities by means of measuring the correlation time and applying the Stokes-Einstein equation, Eq. (3-35), the size of the diffusing particles had to be known. To achieve this, the solutions were doped with a suspension of .038 μm diameter latex spheres in dilute concentrations. Since the size of these spheres was large on a molecular scale, the amount of light scattered by them was dominant over the light scattered by the actual liquid. Thus by rearranging Eq. (4-1) and replacing ξ with the radius r, an expression for the viscosity was found,

$$\eta = \frac{k_B T q^2 \tau_c}{6\pi r} . \qquad (4\text{-}2)$$

So a measurement of τ_c for the doped solutions yielded the viscosity. This value was subsequently normalized to known values to account for systematic errors such as the size of the scattering angle and the uncertainty in the particle size.

Finally, by substituting these values into Eq. (4-1) along with measurements of τ_c in the pure solutions, the correlation lengths were readily obtainable.

Chapter 5

DATA ANALYSIS

The contents of this chapter will include the analyzed data that was obtained using the method and procedures discussed in the previous two chapters. The initial quantity of interest is the correlation time, τ_c, measured first in the pure solutions to determine the relaxation times of the concentration fluctuations and then in solutions doped with latex spheres for the purpose of determining the viscosity.

A measurement of τ_c provides information about the temporal behavior of the liquid. Numerical values of τ_c as well as the viscosity and correlation length are presented in Appendix A. Before any results are shown, a brief discussion of some other properties that were of importance in the analysis of the data will be given.

The cumulant ratio C/R is defined by

$$C/R = \frac{K_2}{K_1^2} \tag{5-1}$$

where K_1 and K_2 have been defined in Eq. (3-37). This is an indicator of how exponential a measured correlation function is. As this ratio approaches zero, the function becomes more exponential. Typical values ranged from 0 to 0.15 and were dependent upon the strength of the signal and how clean the sample was.

The signal strength was of concern because it provided an indication of whether the signal measurement was in a homodyne or heterodyne mode. Determination of the signal strength was done by finding the ratio of the

signal to the background (S/B). A value of S/B $\leq$ 0.03 generally corresponded to a pure heterodyne signal. For homodyne detection, it was usually advantageous to obtain the highest S/B possible.

To evaluate how well points in the correlation function agreed with the fit of Eq. (3-37), a chi-squared test[24] was used. Acceptable data usually yielded a value of $\chi^2 \leq 1.0$.

The scattering angle θ was of significance because it determined in part the value of the scattering vector $\vec{q}$. Evaluation of θ was done by first measuring the angle external to the cell and then using Snell's law to arrive at the angle in the scattering volume. An average value of 1.365 was used for the index of refraction for the TBA-water solutions. The uncertainty in θ was estimated to be no more than $\pm 0.3^{o}$.

The incident wavelength λ was also a determining factor in the scattering vector. With the exception of a small portion of the viscosity data taken at λ = 632.8 nm, all data was measured with λ = 514.5 nm.

The temperature of the cell holder which was being monitored by the thermistor had two main sources of uncertainty. The stability of the temperature was mentioned in Chapter 4, but there was also an uncertainty in reading the DC bridge. Both effects considered, the uncertainty was estimated to be about 0.4^{o}C. A test was conducted to see if the temperature at the sample location agreed with the thermistor. The temperature at the location of the sample was measured with a mercury thermometer. Measurements were taken at -4.0^{o}C, 22.2^{o}C and 55.0^{o}C. After emergent stem corrections were made to the thermometer[25] readings, they were in agreement with the thermistor readings to within the uncertainty.

The correlation times for the pure TBA-water solutions were the first measurements taken. Since the viscosity of a liquid can be described by

the Vogel-Tammann-Fulcher (VTF) equation

$$\eta = \eta_0 \exp\left(\frac{A}{T-T_0}\right), \tag{5-2}$$

where η_0, A, and T_0 are fitting parameters, it was thought that perhaps the correlation times could also be fit to such an equation. The form of the VTF equation would be

$$\tau_c = \tau_0 \exp\left(\frac{A}{T-T_0}\right). \tag{5-3}$$

Table 5-1a lists the best fit parameter for each solution. The data is presented in Figs. 5-1 through 5-5. The solid line in each figure corresponds to values generated by the best fit VTF equation.

To determine the viscosities, some of the solutions were doped with 0.038 μm diameter latex spheres and τ_c was measured. Knowing the radius of the diffusing particles, Eqs. (3-34) and (3-35) yield the viscosity from τ_c. To correct for any systematic errors in the sphere diameter and the scattering angle, the calculated viscosities were normalized to viscosities taken from a graph produced by flow measurements. This method was used for $X_{TBA} = 0.0725$, $X_{TBA} = 0.132$, and $X_{TBA} = 0.201$. Flow measurements were used for $X_{TBA} = 0.152$, and for $X_{TBA} = 0.260$ extrapolations were taken from the flow measurement graph mentioned above. The viscosities for each solution were fit to the VTF equation and the fit parameters are given in Table 5-1b. Results are shown in Figures 5-6 through 5-10.

The scatter in the data appeared to be independent of the temperature or the solution concentration. However, the majority of correlation times were estimated to have an error of less than $\sim\pm 4\%$, derived from the scatter in the data. This applies to both the data taken with pure solutions and with the latex spheres.

With the viscosity and correlation time known, it was possible to determine a correlation length ξ by using the Stokes-Einstein equation,

Table 5-1 FIT PARAMETERS FOR THE VTF EQUATION

TABLE 5-1

Fit Parameters of the Vogel-Tammann-Fulcher Equation for Viscosity and Correlation Time

a. Viscosity

X_{TBA}	$\eta \times 10^{-2}$ (cp)	A(K)	T_o(K)
0.0725	4.447	406.9	199
0.132	6.445	384.4	203
0.152	3.151	542.3	186
0.201	2.597	603.6	181
0.260	1.384	766.1	167

b. Correlation Time

X_{TBA}	τ_o(μsec)	A(K)	T_o(K)
0.0725	0.6726	109.1	242
0.132	0.4527	258.5	216
0.152	0.3473	332.5	200
0.201	0.2836	318.5	210
0.260	0.9173	73.60	266

Figure 5-1 CORRELATION TIME DATA FOR $X_{TBA} = 0.0725$
The line corresponds to value of τ_c determined by the Vogel-Tammann-Fulcher equation with the best fit parameters.

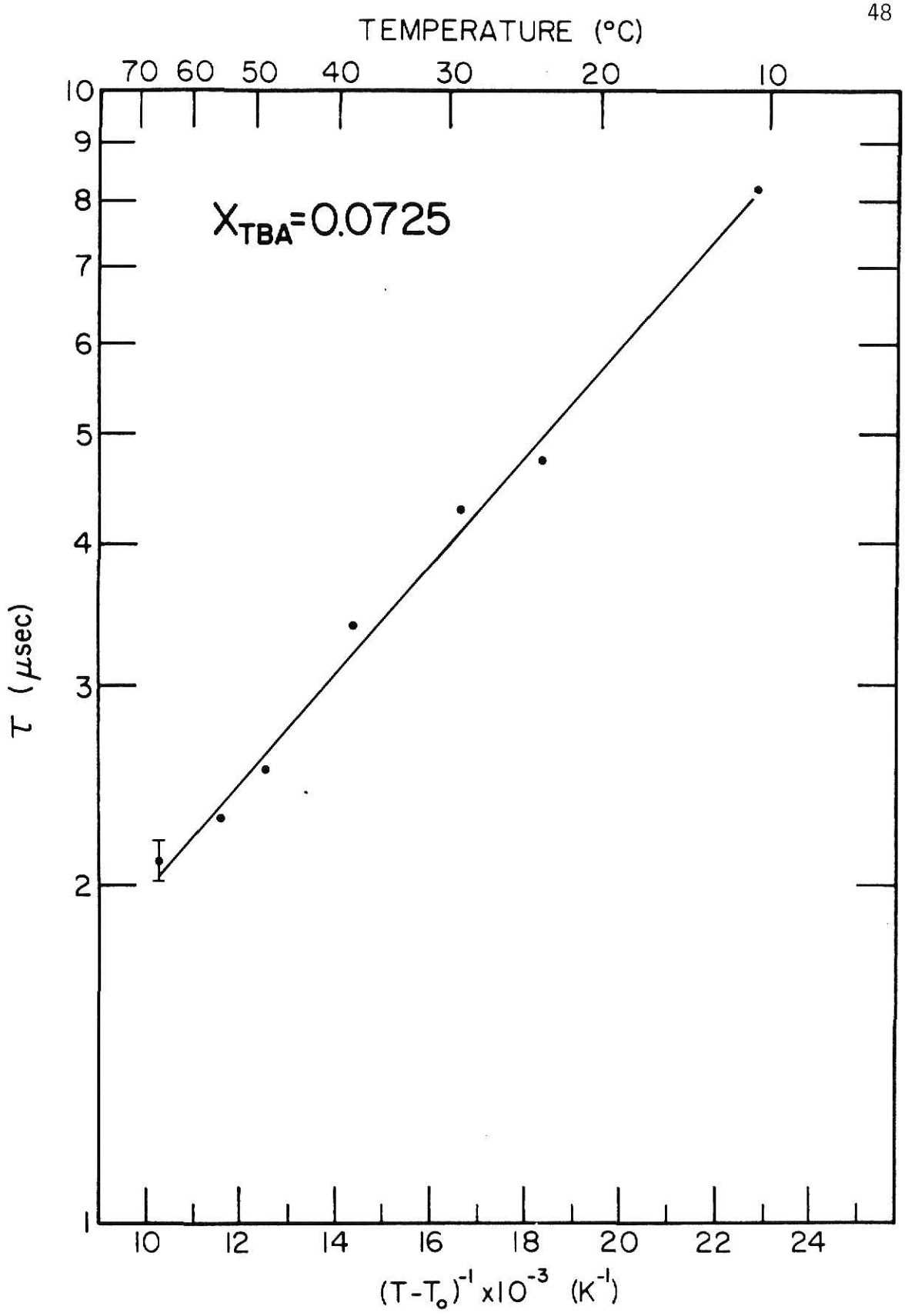
TEMPERATURE (°C)
70 60 50 40 30 20 10
X_{TBA}=0.0725
τ (μsec)
10
9
8
7
6
5
4
3
2
1
10 12 14 16 18 20 22 24
$(T-T_o)^{-1} \times 10^{-3}$ (K^{-1})

Figure 5-2 CORRELATION TIME DATA FOR $X_{TBA} = 0.132$
The line corresponds to value of τ_c determined by the Vogel-Tammann-Fulcher equation with the best fit parameters.

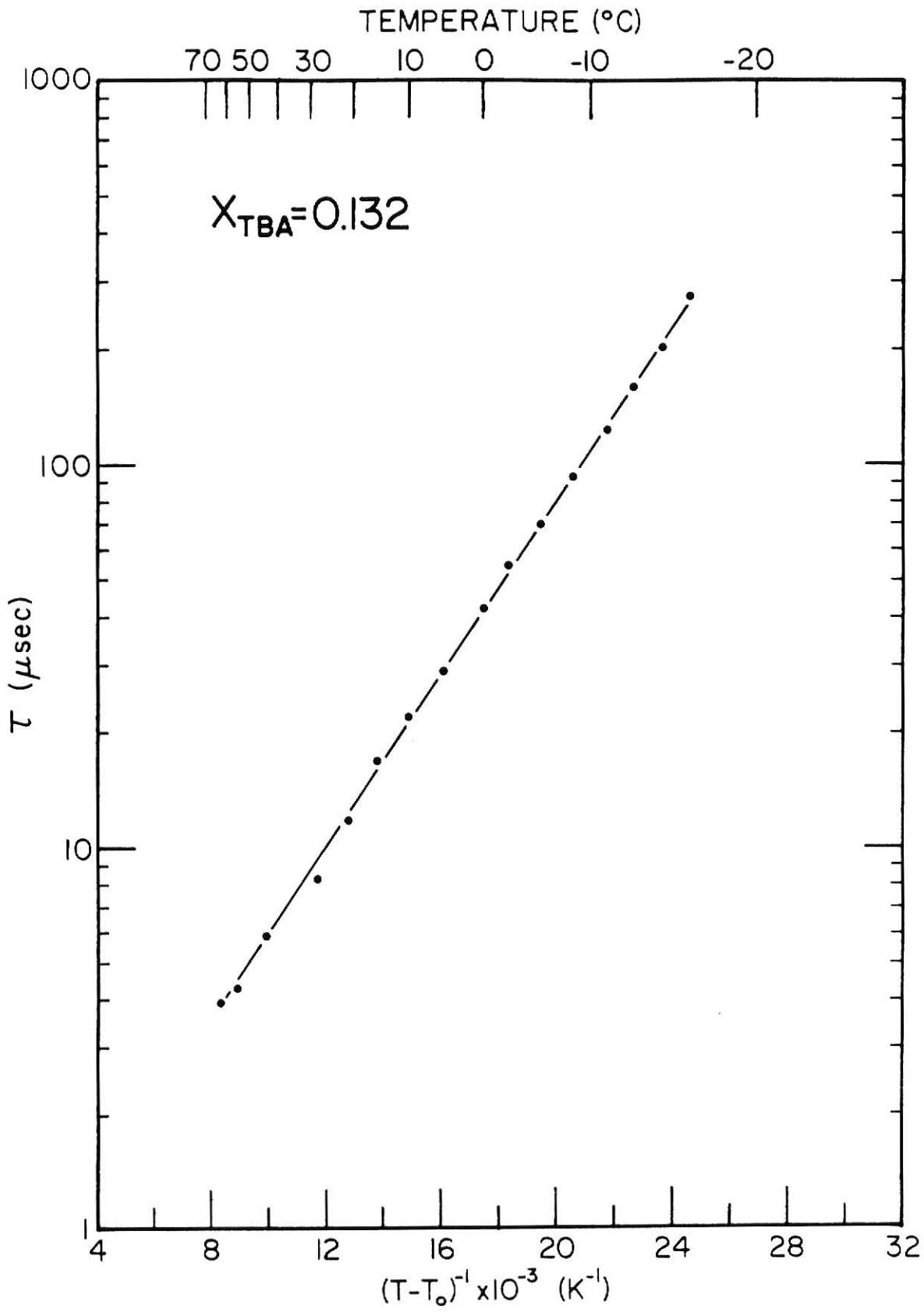
TEMPERATURE (°C)
70 50 30 10 0 -10 -20
1000
100
10
1
X_{TBA}=0.132
τ (μsec)
4 8 12 16 20 24 28 32
$(T-T_o)^{-1} \times 10^{-3}$ (K^{-1})

Figure 5-3 CORRELATION TIME DATA FOR X_{TBA} = 0.152
The line corresponds to value of τ_c determined by the Vogel-Tammann-Fulcher equation with the best fit parameters.

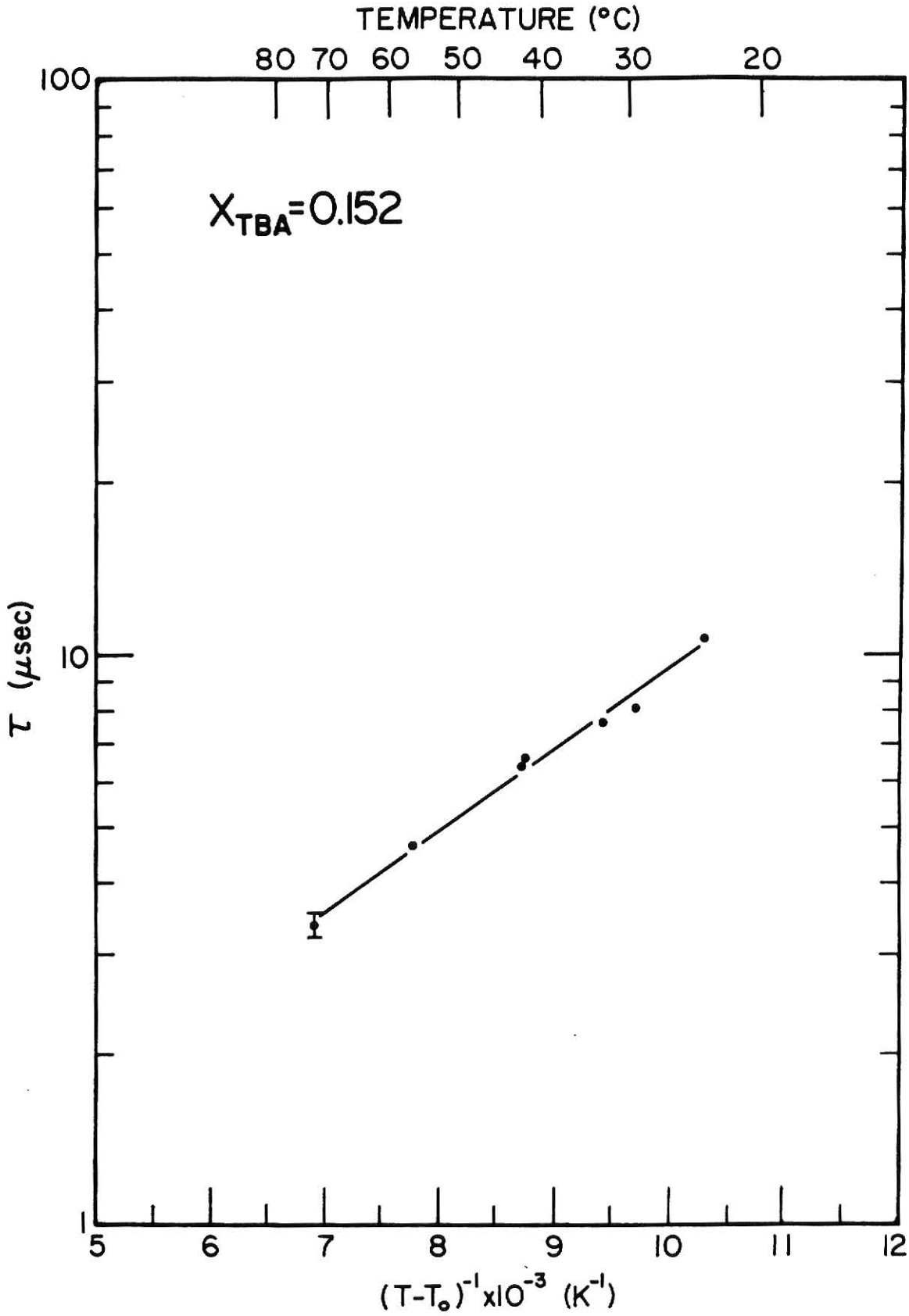
TEMPERATURE (°C)
80 70 60 50 40 30 20
100
10
1
X_{TBA}=0.152
τ (μsec)
5 6 7 8 9 10 11 12
$(T-T_o)^{-1} \times 10^{-3}$ (K^{-1})

Figure 5-4 CORRELATION TIME DATA FOR X_{TBA} = 0.201
The line corresponds to value of τ_c determined by the Vogel-Tammann-Fulcher equation with the best fit parameters.

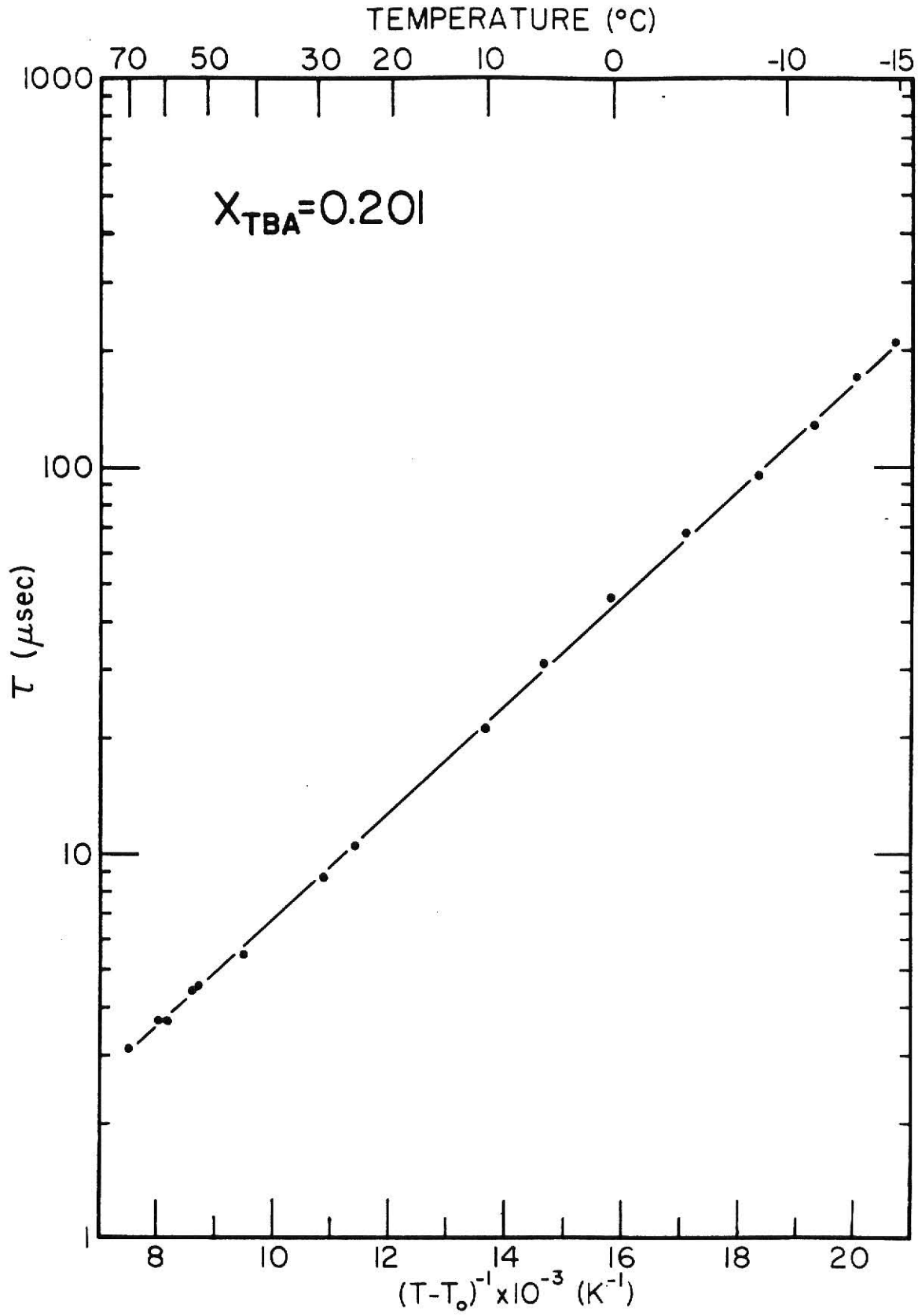
TEMPERATURE (°C)
70
50
30
20
10
0
-10
-15
1000
100
10
1
X_{TBA}=0.201
τ (μsec)
8
10
12
14
16
18
20
$(T-T_o)^{-1} \times 10^{-3}$ (K^{-1})

Figure 5-5 CORRELATION TIME DATA FOR X_{TBA} = 0.260
The line corresponds to value of τ_c determined by the Vogel-Tammann-Fulcher equation with the best fit parameters.

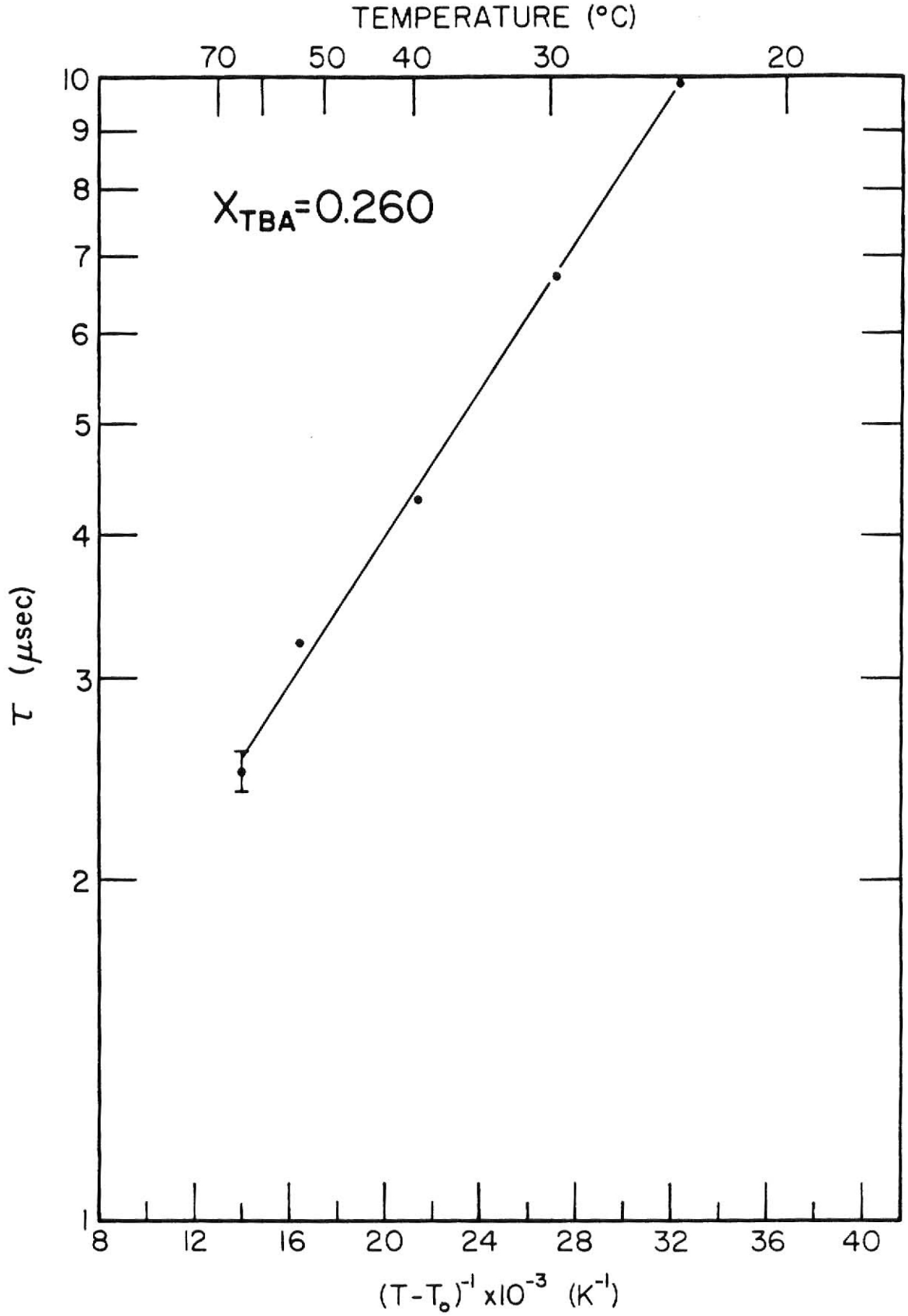
TEMPERATURE (°C)
70
50
40
30
20
X_{TBA}=0.260
τ (μsec)
10
9
8
7
6
5
4
3
2
1
8
12
16
20
24
28
32
36
40
$(T-T_o)^{-1} \times 10^{-3}$ (K^{-1})

Figure 5-6 VISCOSITY DATA FOR $X_{TBA} = 0.0725$

The line corresponds to the values of η determined by the Vogel-Tammann-Fulcher equation with the best fit parameters.

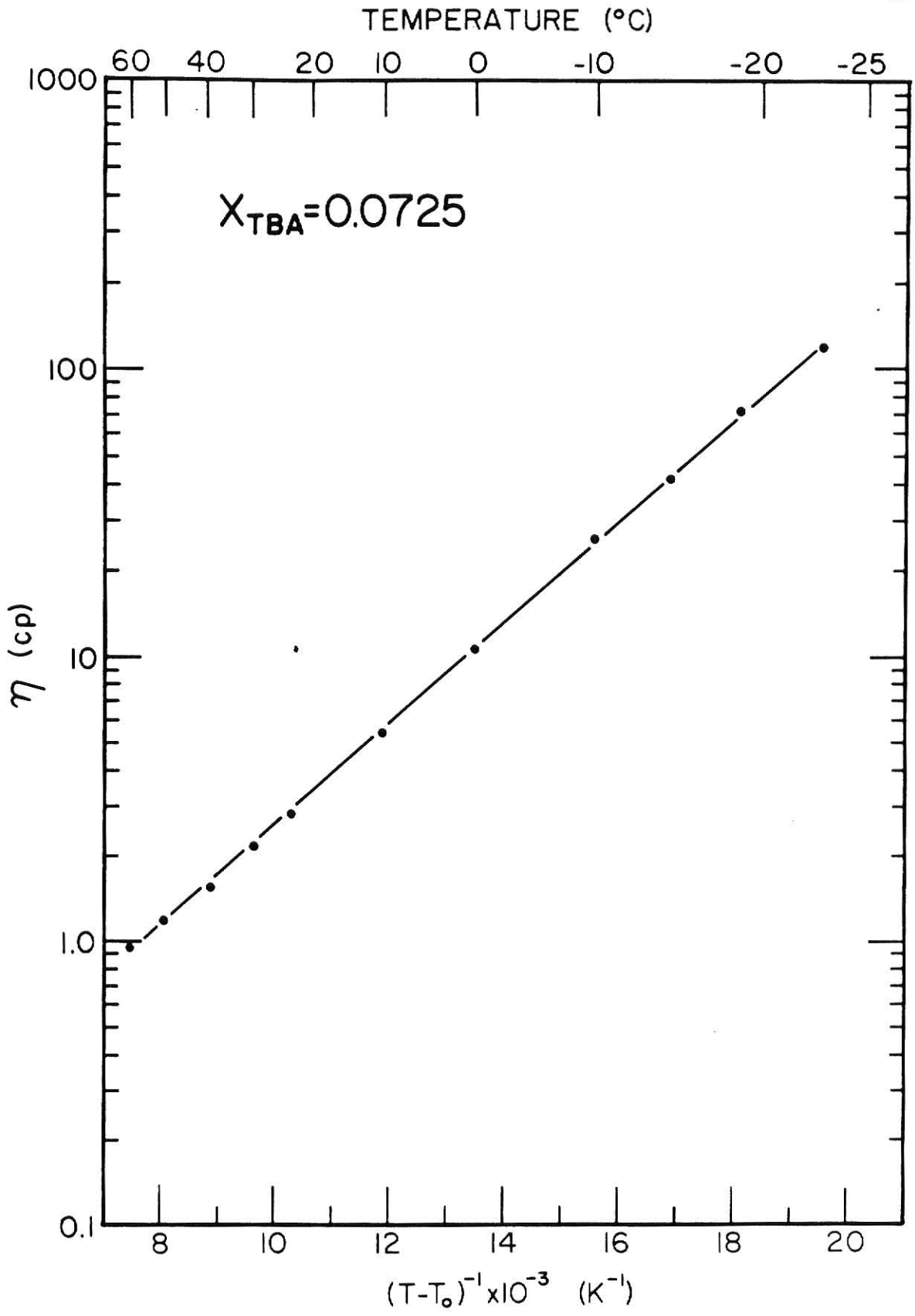
TEMPERATURE (°C)
60
40
20
10
0
-10
-20
-25
1000
100
10
1.0
0.1
X_{TBA}=0.0725
η (cp)
8
10
12
14
16
18
20
$(T-T_o)^{-1} \times 10^{-3}$ (K^{-1})

Figure 5-7 VISCOSITY DATA FOR X_{TBA} = 0.132

The line corresponds to the values of η determined by the Vogel-Tammann-Fulcher equation with the best fit parameters.

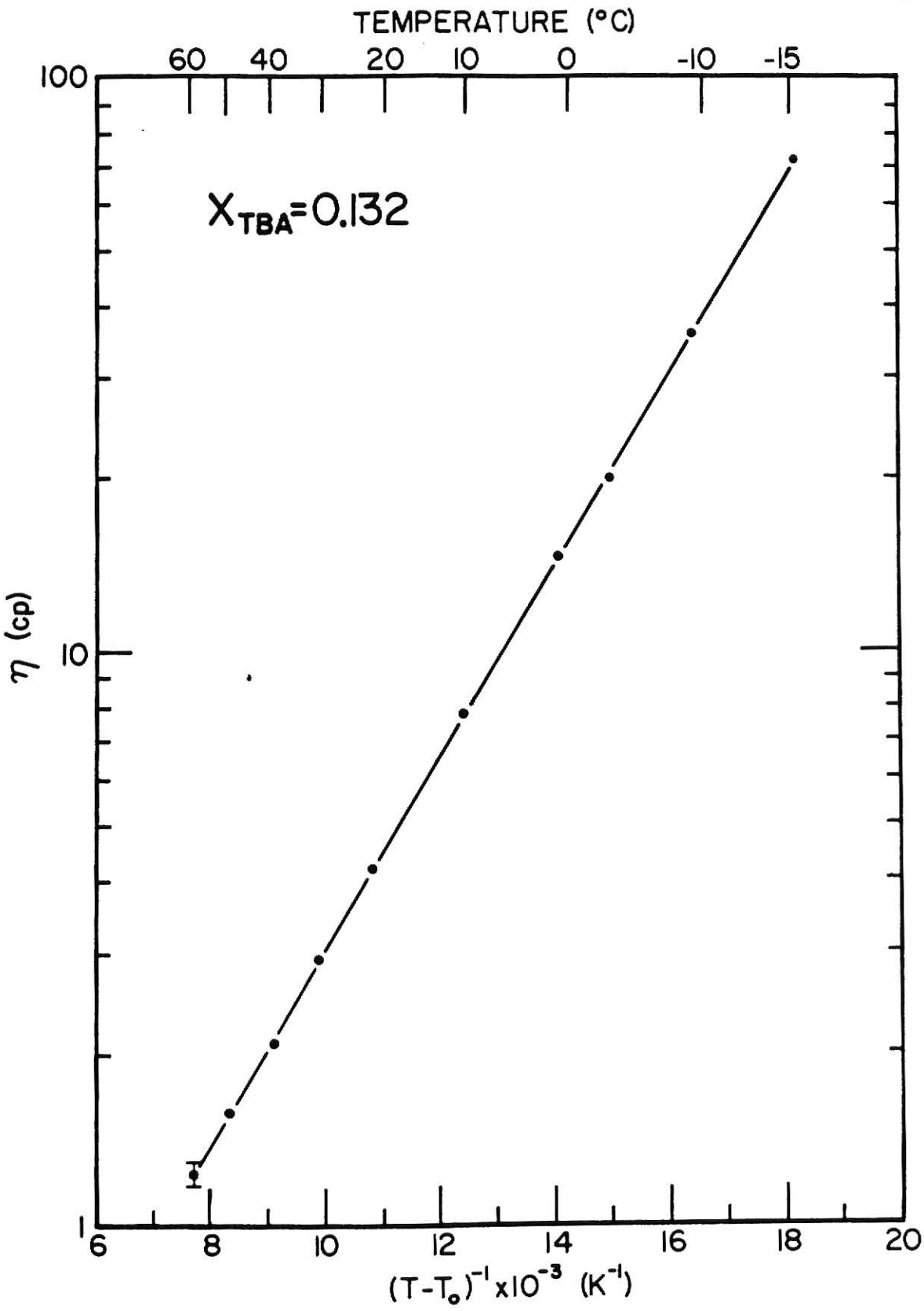
TEMPERATURE (°C)
60
40
20
10
0
-10
-15
100
10
1
X_{TBA}=0.132
η (cp)
6
8
10
12
14
16
18
20
$(T-T_o)^{-1} \times 10^{-3}$ (K^{-1})

Figure 5-8 VISCOSITY DATA FOR X_{TBA} = 0.152

The line corresponds to the values of η determined by the Vogel-Tammann-Fulcher equation with the best fit parameters.

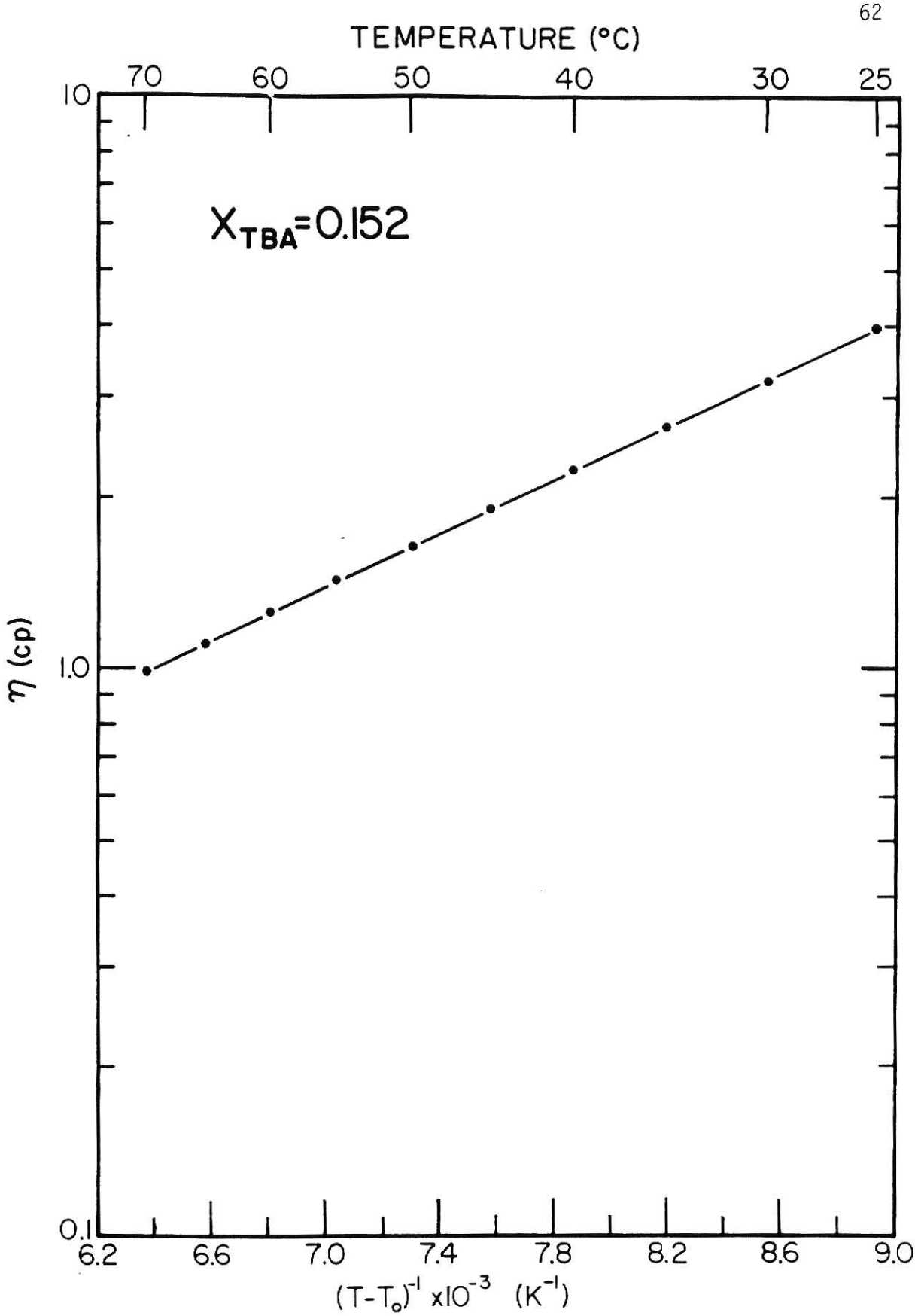
TEMPERATURE (°C)
70
60
50
40
30
25
10
1.0
0.1
X_{TBA}=0.152
η (cp)
6.2
6.6
7.0
7.4
7.8
8.2
8.6
9.0
$(T-T_o)^{-1} \times 10^{-3}$ (K^{-1})

Figure 5-9 VISCOSITY DATA FOR X_{TBA} = 0.201

The line corresponds to the values of η determined by the Vogel-Tammann-Fulcher equation with the best fit parameters.

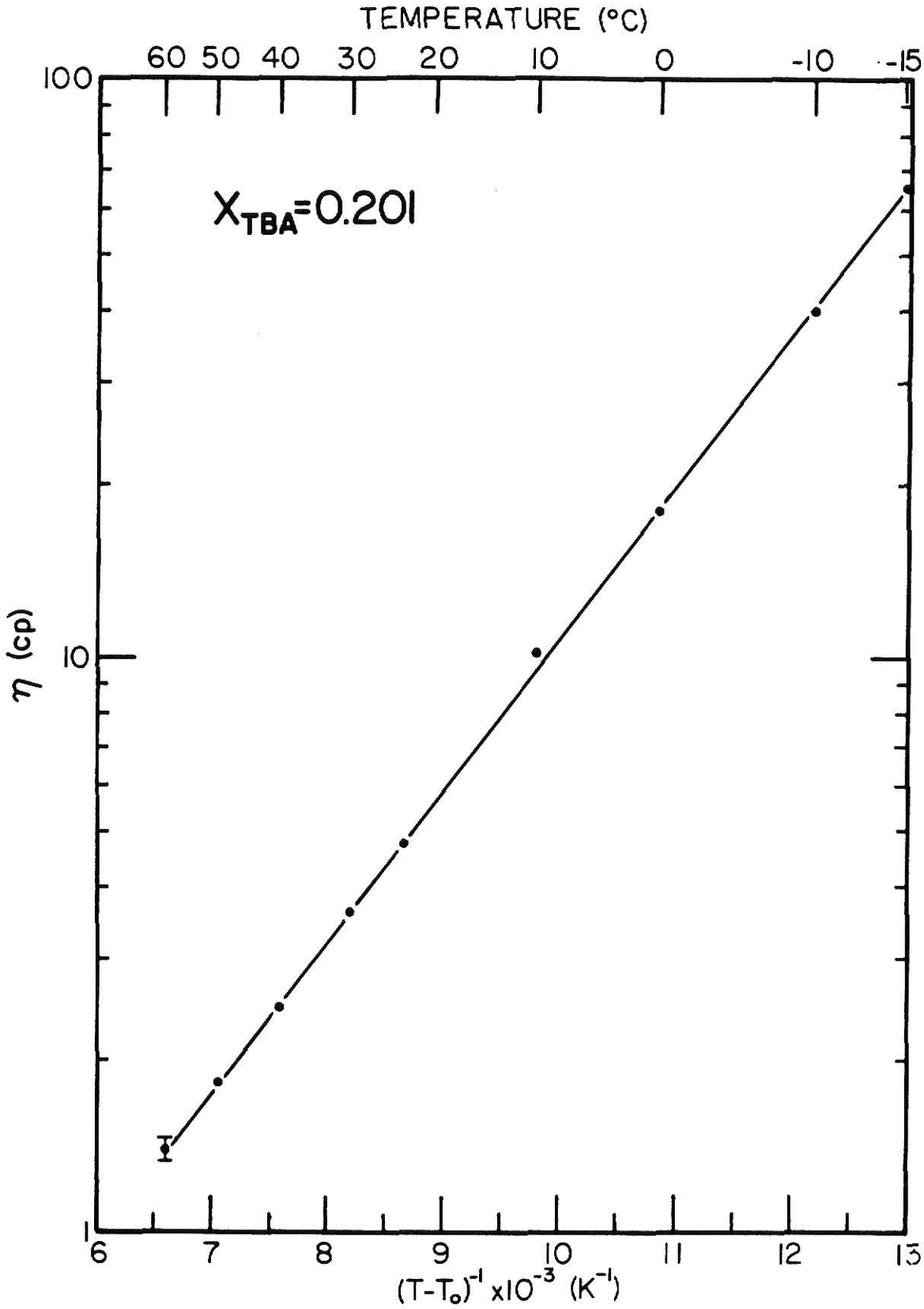
TEMPERATURE (°C)
60 50 40 30 20 10 0 -10 -15
100
10
1
X_{TBA}=0.201
η (cp)
6 7 8 9 10 11 12 13
$(T-T_o)^{-1} \times 10^{-3}$ (K^{-1})

Figure 5-10 VISCOSITY DATA FOR X_{TBA} = 0.260

The line corresponds to the values of η determined by the Vogel-Tammann-Fulcher equation with the best fit parameters.

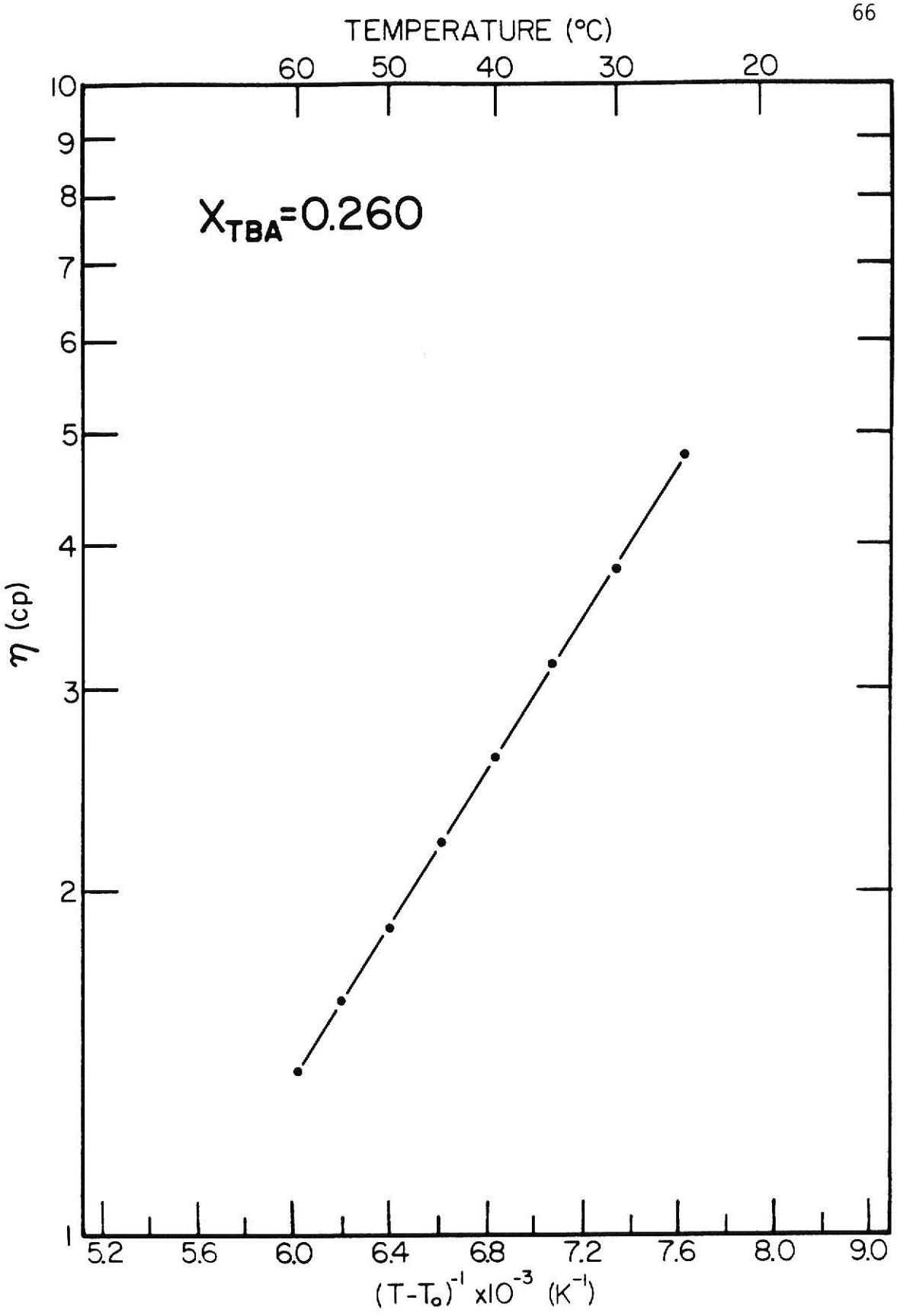
TEMPERATURE (°C)
60
50
40
30
20
10
9
8
7
6
5
4
3
2
1
X_{TBA}=0.260
η (cp)
5.2
5.6
6.0
6.4
6.8
7.2
7.6
8.0
9.0
$(T-T_o)^{-1} \times 10^{-3}$ (K^{-1})

$$\frac{1}{\tau_c q^2} = \frac{K_B T}{6\pi\eta\xi}. \qquad (5\text{-}4)$$

The vicosity corresponding to a temperature at which a correlation time was measured came directly from the VTF equation of η for that solution. The correlation lengths are listed in Appendix A and the temperature dependence can be seen in Figures 5-11 through 5-15. The boiling temperature for a solution of intermediate concentration was measured at $\sim 73^{o}C$. Above this temperature, solutions may have undergone rapid evaporation causing the concentration to change. Thus, values of ξ above $\sim 73^{o}C$ may be inaccurate.

Another approach that was taken involved calculating ξ by using values of τ_c from the VTF equation. This allowed extrapolations of τ_c beyond the experimental limitations, i.e. above the boiling point and below the temperature at which the sample nucleated. The extrapolations of τ_c and η then lead to a prediction of how the correlation length might behave in these extreme regions. Figure 5-16 shows the results of such calculations. In the figure, the solid lines represent points within the range of data used to fit the VTF equation and the dashed lines correponds to points outside of this range.

Certainly for the cases of X_{TBA} = 0.0725, 0.152, and 0.260, the accuracy of the extrapolations might be questionable for more than a few degrees in temperature. However, for X_{TBA} = 0.132 and 0.201, the VTF equation for τ_c was fit over ranges of $80^{o}C$ and $85^{o}C$ respectively while the fit for η spanned approximately $75^{o}C$ for both solutions. Thus an accurate extrapolation for several degrees beyond the actual data should be possible in these two instances.

A qualitative observation made on the intensity of the scattered light is worth mentioning here. In the high temperature region, the intensity decreased as the temperature was lowered. Lowering the temperature

Figure 5-11 CORRELATION LENGTH DATA FOR $X_{TBA} = 0.0725$

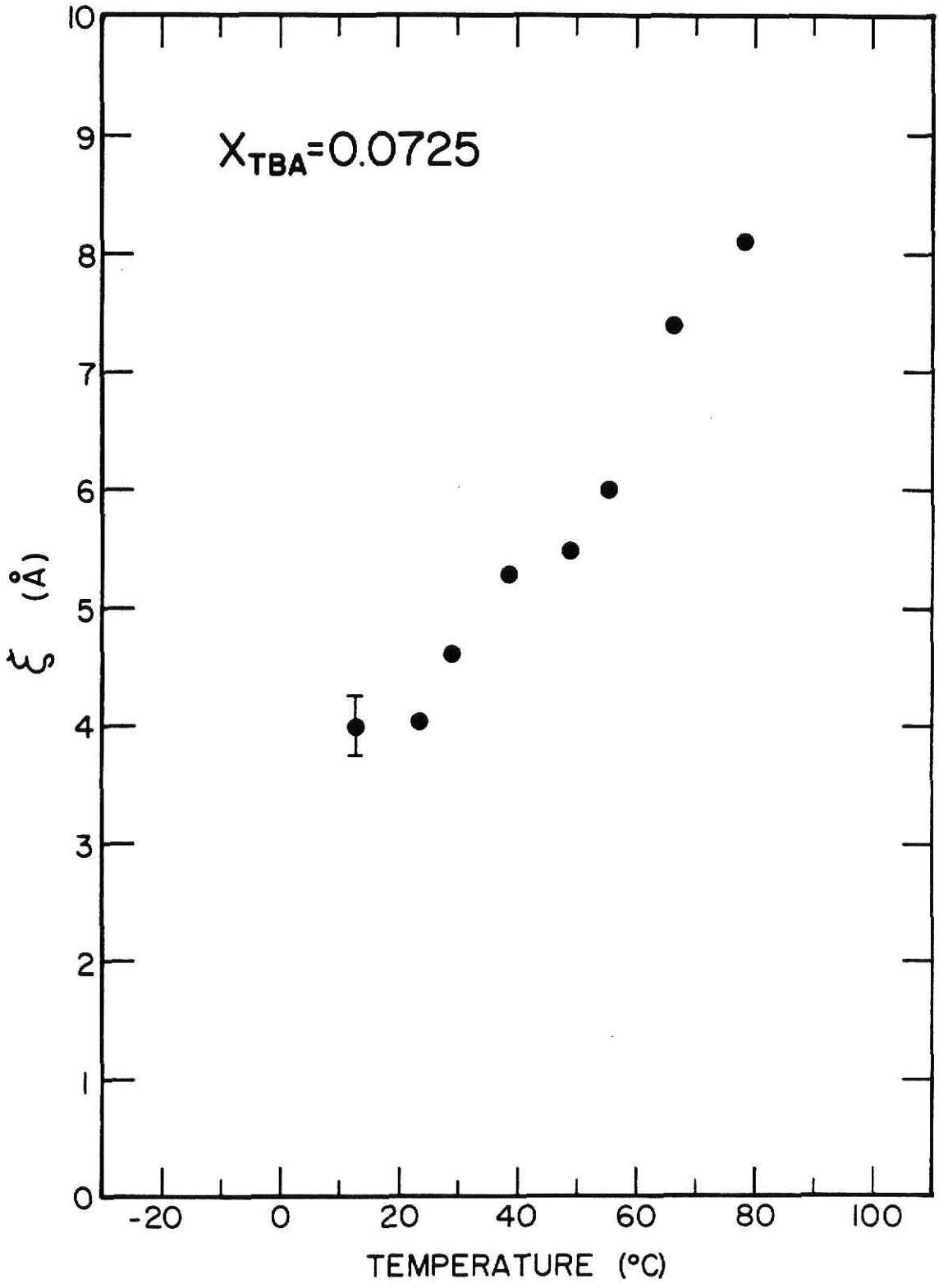
X_{TBA}=0.0725
ξ (Å)
TEMPERATURE (°C)
0
1
2
3
4
5
6
7
8
9
10
-20
0
20
40
60
80
100

Figure 5-12 CORRELATION LENGTH DATA FOR $X_{TBA} = 0.132$

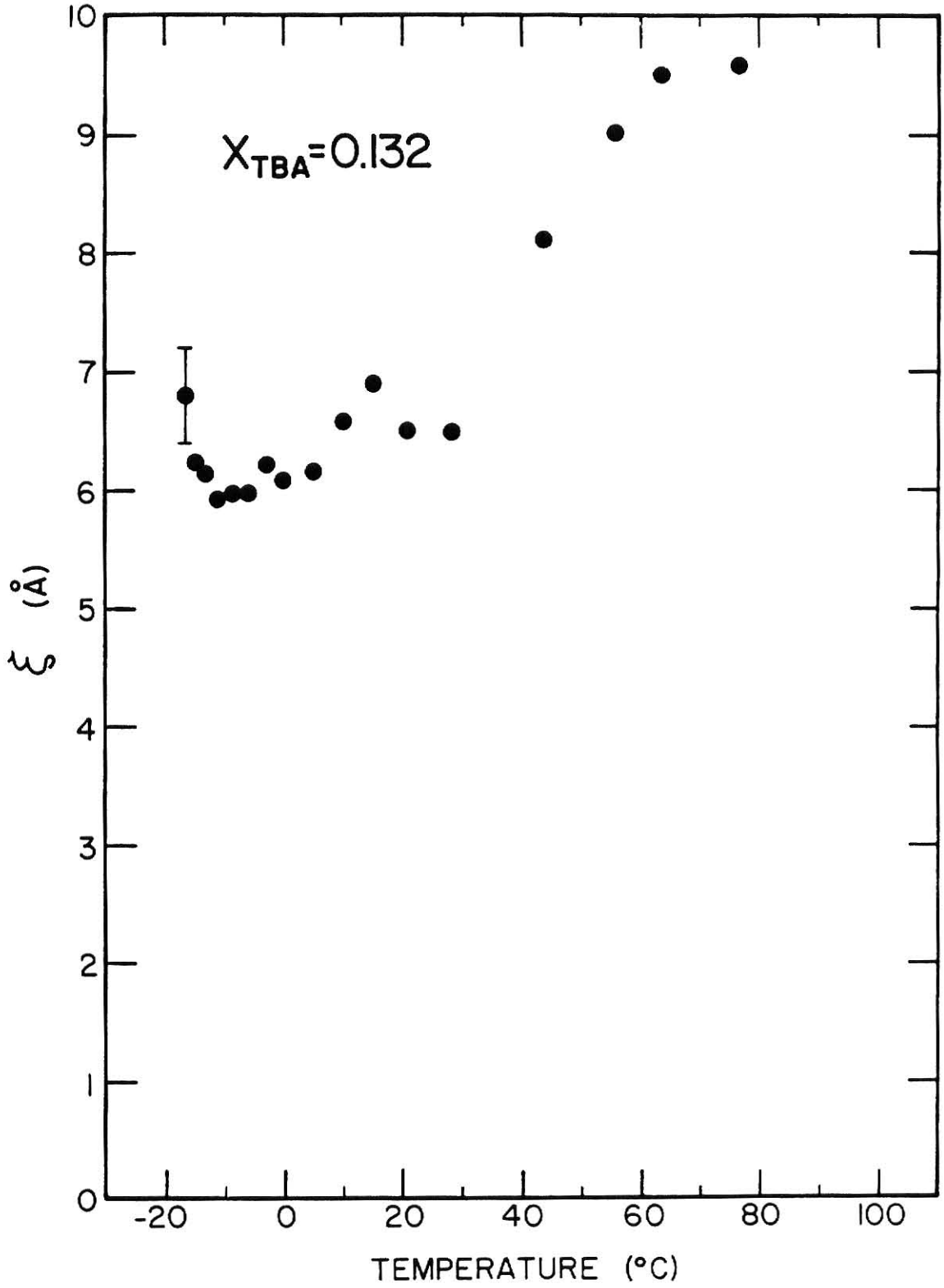
X_{TBA}=0.132
ξ (Å)
TEMPERATURE (°C)
0
1
2
3
4
5
6
7
8
9
10
-20
0
20
40
60
80
100

Figure 5-13 CORRELATION LENGTH DATA FOR $X_{TBA} = 0.152$

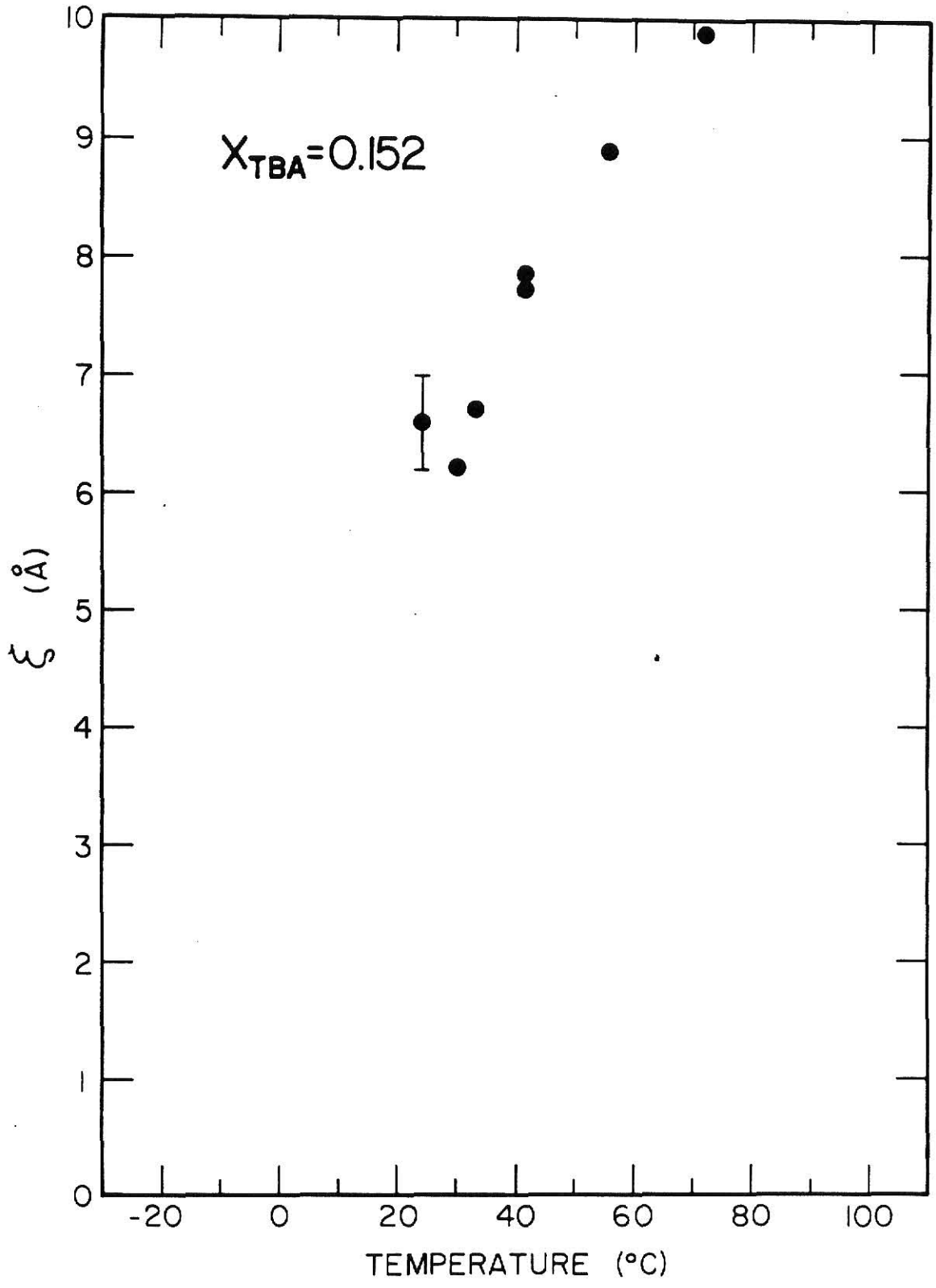
X_{TBA}=0.152
ξ (Å)
TEMPERATURE (°C)
0
1
2
3
4
5
6
7
8
9
10
-20
0
20
40
60
80
100

Figure 5-14 CORRELATION LENGTH DATA FOR X_{TBA} = 0.201

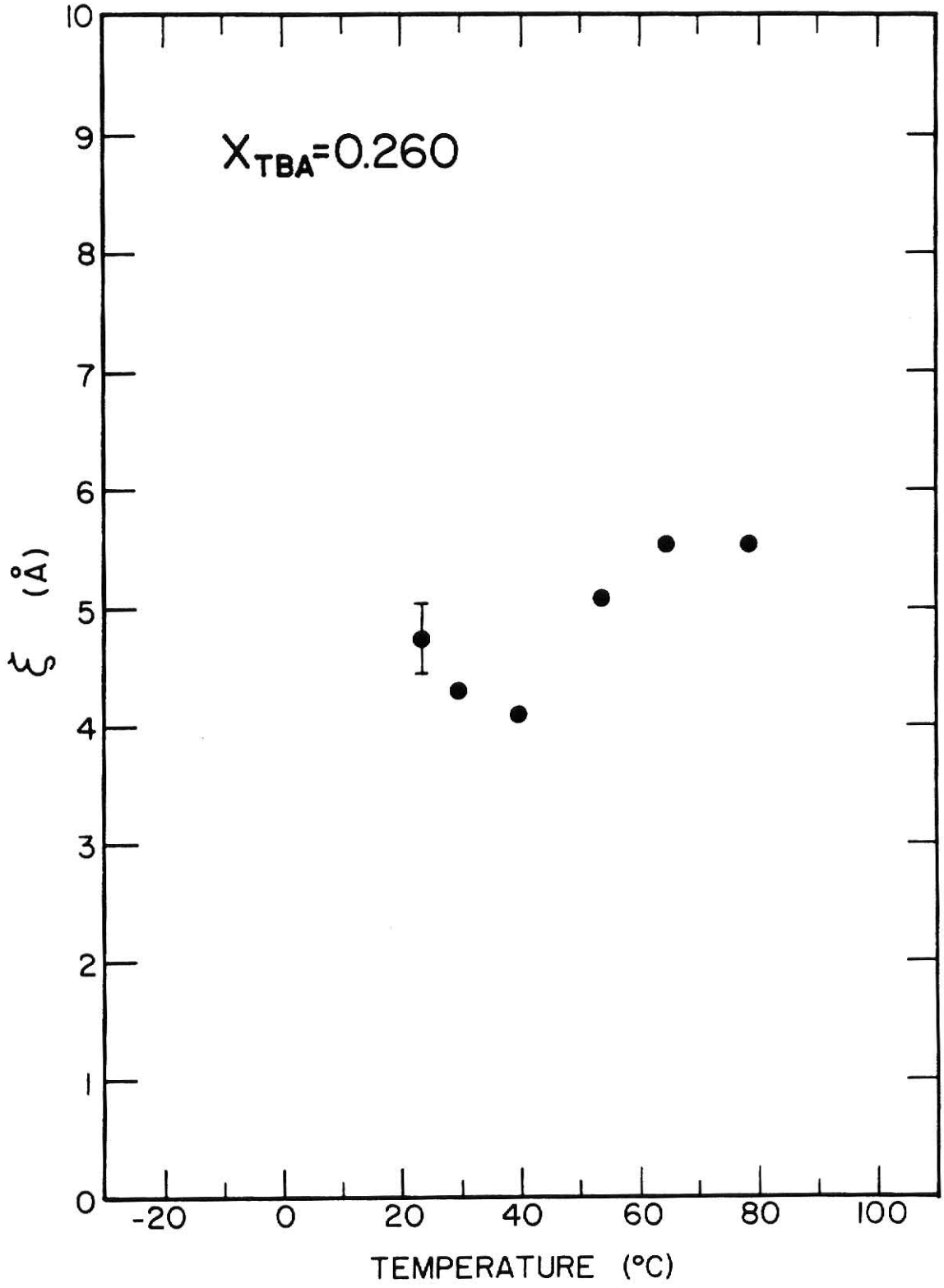
X_{TBA}=0.260
ξ (Å)
TEMPERATURE (°C)
0
1
2
3
4
5
6
7
8
9
10
-20
0
20
40
60
80
100

Figure 5-15 CORRELATION LENGTH DATA FOR X_{TBA} = 0.260

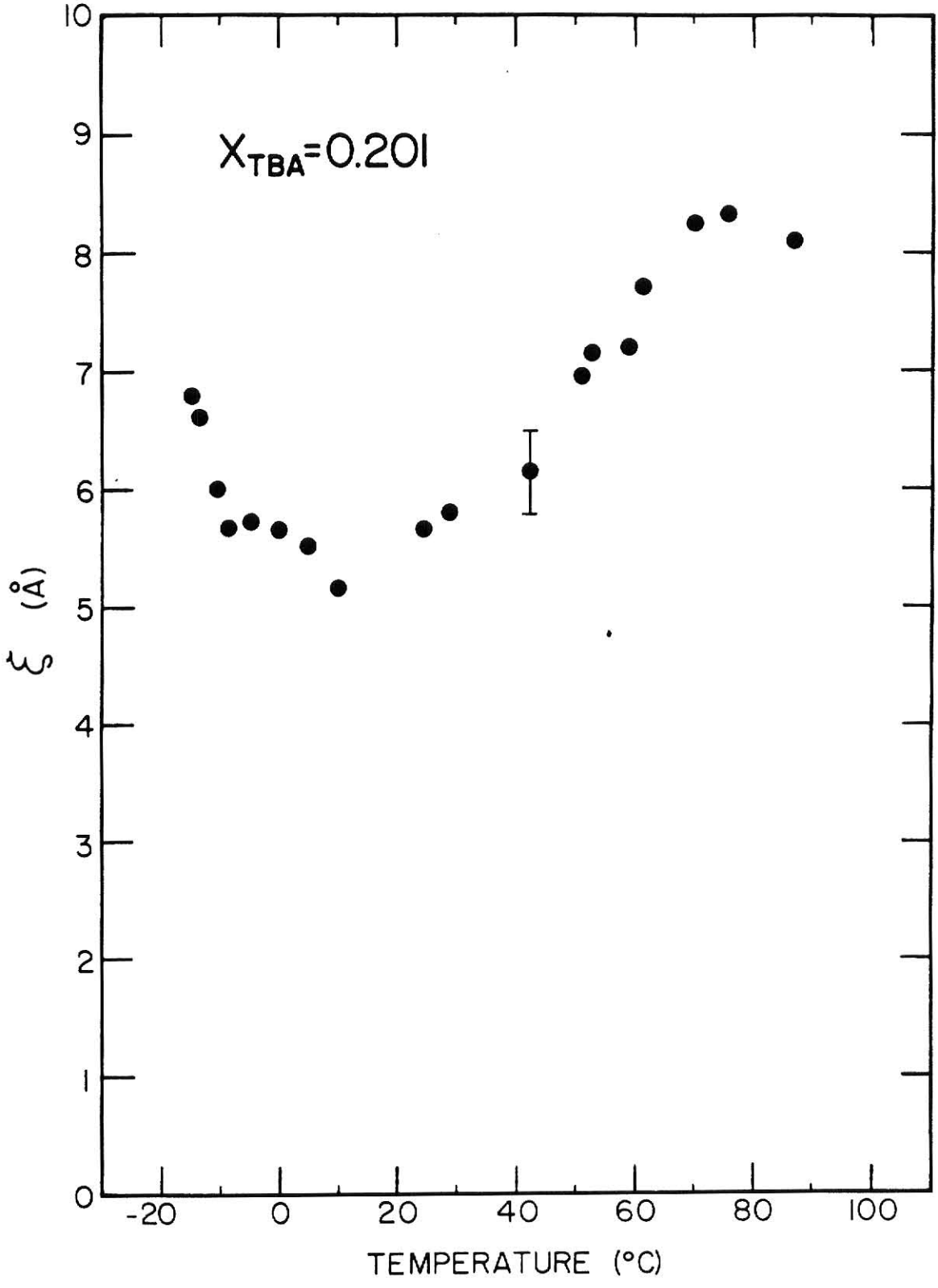
X_{TBA}=0.201
ξ (Å)
TEMPERATURE (°C)
0
1
2
3
4
5
6
7
8
9
10
-20
0
20
40
60
80
100

Figure 5-16 COMPUTED CORRELATION LENGTHS

This figure represents the values of ξ computed by using values of η and τ_c obtained with the VTF equation. The dashed lines correspond to extrapolations of η and/or τ_c beyond the temperature range in which actual data was acquired.

Line	X_{TBA}
A	0.152
B	0.132
C	0.201
D	0.0725
E	0.260

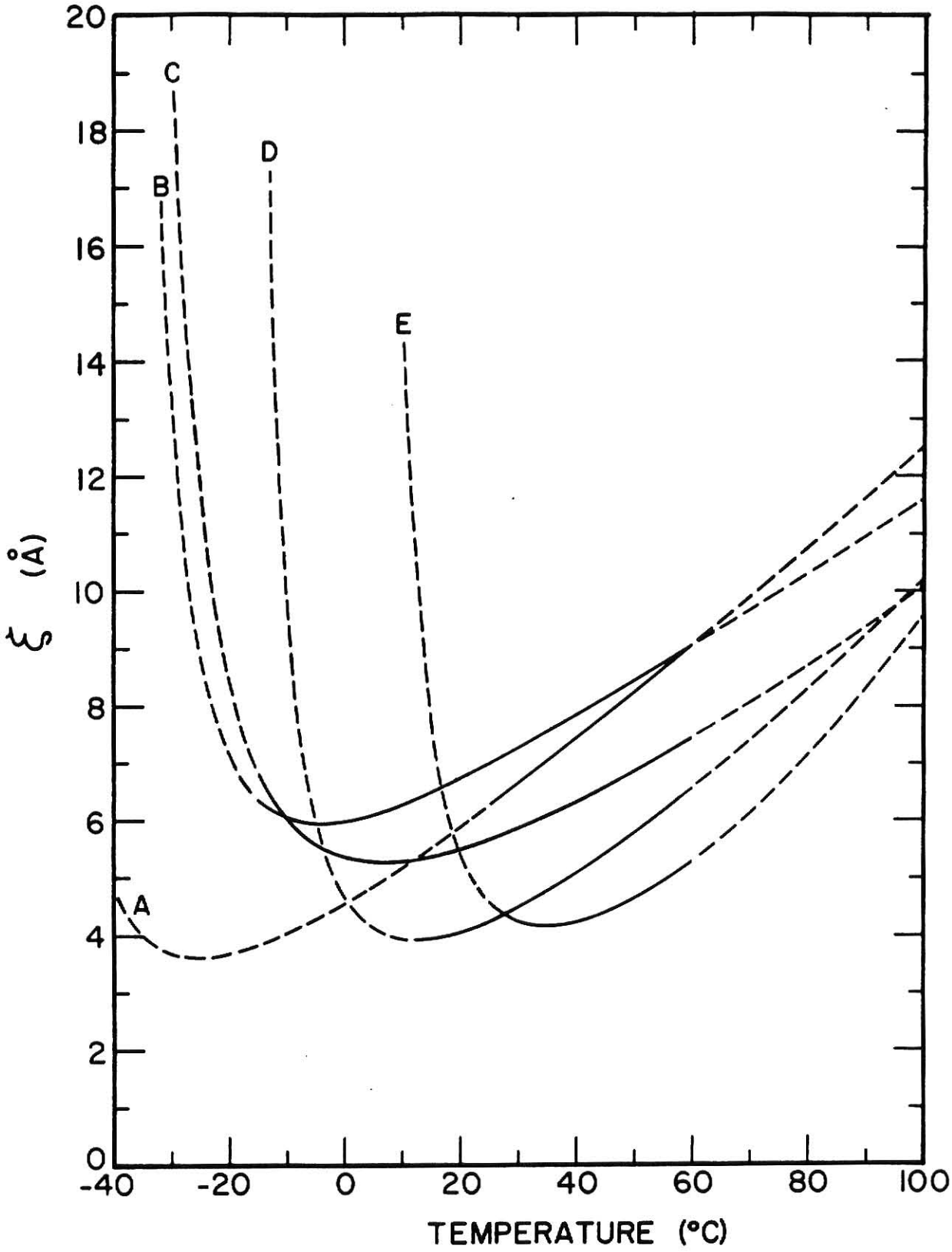
20
18
16
14
12
10
8
6
4
2
0
ξ (Å)
A
B
C
D
E
-40
-20
0
20
40
60
80
100
TEMPERATURE (°C)

further, however, caused the intensity of the scattered light to increase in the low temperature region. This was seen in the X_{TBA} = 0.132 and 0.201 solutions for which low temperature data was obtained. This supports the results concerning ξ since an increase in the size of the fluctuations will cause an increase in the scattering intensity. In addition, the approximate temperature region where the intensity begins increasing agrees with the region where ξ begins increasing.

Another observation observed which should be pointed out was made while attempting to obtain low temperature data for X_{TBA} = 0.0725. What appeared to be some type of precipitate seemed to be forming in the solution. This produced unusually high intensity scattering and long correlation times corresponding to particles with diameters on the order of 0.25 μm. Therefore data was not obtained in this region.

Chapter 6

DISCUSSION OF RESULTS AND CONCLUSIONS

The results displayed in Figs. 5-11 through 5-16 clearly show that as the temperature is lowered, the correlation length decreases initially. At some temperature the diminishment in ξ appears to cease. This temperature, as well as its value of ξ, seems to be dependent upon the concentration of the solution. For the solutions where enough low temperature data are available, an increase in ξ is seen to start taking place as the temperature is lowered further. The same behavior is predicted for the other concentrations by the extrapolations in Fig. 5-17.

The maximum correlation length for solutions at room temperature (and above) appears to lie in the concentration range around $X_{TBA} = 0.132$. This is supportive of results from x-ray scattering, ultrasonic absorption, and light scattering intensity measurements made by others.[16,17,18] However the size indicated here is slightly smaller than what some have measured.[16] The high temperature behavior of ξ is compatible with published results[23] on the temperature dependence of the scattering intensity for aqueous TBA solutions.

In an effort to explain some of the behavior exhibited, consider the high temperature region where ξ is increasing as the temperature rises. TBA + H_2O is known to be a non-ideal solution. That means that a single state of mixing might not exist for all concentrations at all temperatures. This has led to the suggestion that a lower critical solution temperature (LCST) might be present somewhere above the boiling point.

Near a LCST the correlation length becomes divergent similar to when the critical point in a liquid-gas system is approached. At the LCST, ξ becomes infinite and the system undergoes a second-order phase transition. The increasing trend seen in ξ at high temperatures for the TBA-water systems seems to indicate the possibility of a LCST. H.-D. Ludemann was able to find such a critical solution temperature in solutions of TBA and water mixed with KCl. However as the concentration of KCl was diminished, the LCST vanished before $X_{KCl} = 0$. Interesting behavior is exhibited not only at a LCST but begins appearing in the region around it. The high temperature increase in ξ seen in the TBA-water solutions may be the remnants of a LCST or an effect from being in the region of a LCST even though the LCST is no longer on the real part of the phase diagram. One might even say that the TBA-water is approaching a "virtual" LCST.

Now consider the low temperature region where ξ stops decreasing and begins to increase as the temperature is lowered. This indicates once again the growth of some type of correlated patches in the structure of the solution. The fact that TBA-water is believed to be a good clathrate former makes it reasonable to assume that these correlated patches are probably liquid clathrates. The extrapolations into the low temperature regions seen in Fig. 5-17 predict a divergence in ξ at some temperature dependent upon the concentration. Such a divergence in ξ would imply a limit of stability in the TBA-water solution and therefore yet another second-order phase transition.

Could the divergence in ξ of TBA-water solutions then be related to the stability limit in pure water proposed by Speedy and Angell[2]? Singular behavior seen in supercooled water was discussed earlier. This behavior is analogous to critical phenomena. The evidence pointing

toward the stability limit in water lies in the singular behavior, in other words in the divergence seen in the various thermodynamic and transport properties. Statistical mechanical arguments have been used[14] to explain these divergences based upon increased fluctuations in the density and the entropy. Measurements of the static structure factor have shown an increase in the length scale of density fluctuations in water as the temperature was decreased.[12] The analogy to critical phenomena, the diverging properties, and the static structure factor measurements all indicate the presence of long range fluctuations in the supercooled water. What type of structure is responsible for these fluctuations? Halfpap and Sorensen[5] have successfully used a clathrate model to explain the divergence of the viscosity. Certainly an increase in the concentration of the open structured clathrates would create an increase in the density and entropy fluctuations, thus making the clathrate model compatible with the results mentioned above.

The increase seen in ξ when the TBA-water solutions were supercooled is a direct indication of an increase in the size of the fluctuations present in the solutions. This increase in ξ along with the ensuing stability limit is coherent with the behavior of the static structure factor[12] and the limit of stability in supercooled water. There is a substantial amount of supportive evidence that TBA induces the formation of clathrates in water. Clathrates are also believed to form more readily at low temperatures, thus reinforcing the idea that clathrate growth is responsible for the low temperature increase of ξ in supercooled TBA-water.

So by dissolving TBA in water, we have deliberately caused the formation of liquid clathrates and, as stated above, have produced behavior similar to that seen in supercooled water. We have concluded that the behavior of the TBA-water solutions was directly caused by clathrates.

Thus, the similarity to the behavior of supercooled water suggests that liquid clathrates are also forming in pure supercooled water, causing an increase in the static structure factor (equivalent to an increasing correlation length) and leading to the limit of stability.

APPENDIX A

Presented here is the viscosity data over a range of temperatures for each solution studied. This is followed by the correlation time data for the pure solutions and the corresponding correlation lengths. The mole fraction of tert-butyl alcohol for each set of data is designated by X_{TBA}. All data was taken with λ=514.5 nm except the viscosity data for X_{TBA} = 0.132 below 20^{o}C where λ=632.8 nm. For all viscosity data, θ=90^{o}. For the correlation time data below 20^{o}C, θ=90^{o}C and at 20^{o}C and above, θ=25.8^{o}.

$X_{TBA} = 0.0725$

Temperature (^{o}C)	τ_c (msec)	η(cp)	Normalized η(cp)*
60.0	0.0730	1.04	0.954
49.9	0.0939	1.30	1.19
40.0	0.126	1.69	1.55
29.9	0.182	2.36	2.16
23.0	0.241	3.06	2.81
9.9	0.492	5.96	5.46
-0.1	1.004	11.7	10.7
-10.0	2.49	28.1	25.8
-15.0	4.36	48.2	44.2
-19.0	7.18	78.2	71.7
-23.0	12.2	130.7	120.0

$X_{TBA} = 0.132$

Temperature (^{o}C)	τ_c (msec)	η(cp)	Normalized η(cp)*
59.9	0.0955	1.36	1.24
49.8	0.126	1.74	1.58
40.0	0.172	2.30	2.09
30.8	0.247	3.22	2.93
22.1	0.363	4.59	4.18
10.3	1.06	8.52	7.75
0.8	2.06	16.0	14.6
-3.5	2.86	21.9	19.9
-9.3	5.25	39.3	35.8
-15.3	10.8	78.9	71.8

* Normalized to flow measurements

$X_{TBA} = 0.201$

Temperature (^{o}C)	τ_c (msec)	η(cp)	Normalized η(cp)*
59.9	0.104	1.48	1.39
49.9	0.141	1.95	1.83
40.0	0.197	2.64	2.47
29.9	0.297	3.85	3.61
23.3	0.400	5.08	4.76
9.9	0.881	10.7	10.02
0.0	1.63	19.1	17.9
-10.0	3.78	42.6	39.9
-15.0	6.30	69.7	65.3

* Normalized to flow measurements

$X_{TBA} = 0.152$

Temperature (^{o}C)	n(cp)**
70	0.992
65	1.11
60	1.26
55	1.43
50	1.64
45	1.91
40	2.24
35	2.67
30	3.22
25	3.97

$X_{TBA} = 0.260$

Temperature (^{o}C)	n(cp)**
60	1.39
55	1.61
50	1.86
45	2.21
40	2.62
35	3.15
30	3.81
25	4.78

** Flow measurements of viscosity

$X_{TBA} = 0.0725$

Temperature (°C)	τ_c(μsec)	Equivalent τ_c(μsec)***	ξ(Å)
78.8	36.1	1.80	8.14
66.8	42.3	2.11	7.36
55.6	46.0	2.29	6.02
49.0	50.7	2.53	5.51
38.6	68.0	3.39	5.27
29.1	85.7	4.27	4.62
23.4	95.2	4.74	4.00
12.6	8.20	8.20	3.97

$X_{TBA} = 0.132$

Temperature (°C)	τ_c(μsec)	Equivalent τ_c(μsec)***	ξ(Å)
77.2	59.3	2.96	9.64
63.9	79.5	3.96	9.58
56.1	92.0	4.58	9.07
44.0	118.	5.88	8.12
28.5	167.	8.32	6.44
21.0	237.	11.8	6.46
15.3	16.9	16.9	6.85
10.1	22.0	22.0	6.54
5.1	28.9	28.9	6.14
0.0	42.2	42.2	6.07
-2.8	54.8	54.8	6.21
-5.9	70.0	70.0	5.96
-8.7	93.2	93.2	5.98
-11.3	123.	123.	5.92
-13.2	160.	160.	6.15
-14.9	201.	201.	6.24
-16.6	276.	276.	6.82

$X_{TBA} = 0.152$

Temperature (°C)	τ_c (μsec)	Equivalent τ_c (μsec)***	ξ (Å)
85.1	56.3	2.81	11.2
72.5	67.4	3.36	10.0
55.4	93.2	4.64	8.77
42.0	128.	6.38	7.80
41.7	132.	6.58	7.96
33.5	153.	7.62	6.74
30.2	162.	8.07	6.22
24.2	224.	11.2	6.60

$X_{TBA} = 0.201$

Temperature (°C)	τ_c (μsec)	Equivalent τ_c (μsec)***	ξ (Å)
87.8	41.4	2.06	8.14
76.4	55.2	2.75	8.39
70.7	62.7	3.12	8.26
62.0	74.4	3.71	7.76
59.7	74.1	3.69	7.23
53.2	89.8	4.48	7.20
51.7	91.5	4.56	6.99
42.7	110.	5.48	6.17
29.1	178.	8.87	5.79
24.6	213.	10.6	5.62
10.1	21.2	21.2	5.14
5.1	31.2	31.2	5.48
0.0	46.1	46.1	5.64
-4.7	67.6	67.6	5.72
-8.7	94.8	94.8	5.68
-11.3	128.	128.	6.01
-13.2	170.	170.	6.62
-14.9	208.	208.	6.80

$X_{TBA} = 0.260$

Temperature (°C)	τ_c (μsec)	Equivalent τ_c (μsec)***	ξ (Å)
79.3	35.3	1.76	5.86
65.1	49.7	2.48	5.63
53.9	64.6	3.22	5.16
39.7	85.8	4.28	4.12
29.7	137.	6.83	4.32
23.8	198.	9.87	4.74

***The equivalent correlation time for a homodyne signal at a 90° scattering angle.

REFERENCES

1. C. A. Angell, J. Shuppert, and J. C. Tucker, J. Chem. Phys. 77, 3092 (1973).
2. R. J. Speedy and C. A. Angell, J. Chem. Phys. 65, 851 (1976).
3. J. Hallett, Proc. Phys. Soc. 82, 1046 (1963).
4. M. Oguni and C. A. Angell, J. Chem. Phys. 73, 1948 (1980).
5. B. L. Halfpap and C. M. Sorensen, J. Chem. Phys. 77, 466 (1982).
6. R. J. Speedy, J. A. Ballance, and B. D. Cornish, J. Phys. Chem. 87, 325 (1983).
7. Hydrogen Bonded Solvent Systems, edited A. K. Covington and P. Jones (Taylor and Francis LTD, Londong, England, 1968).
8. F. H. Stillinger, Science 209, 451 (1980).
9. D. W. Davidson in Water, A Comprehensive Treatise, F. Franks, Ed. (Plenum, New York, 1973) Vol. 2.
10. C. A. Angell in Water, A Comprehensive Treatise, F. Franks, Ed. (Plenum, New York, 1982) Vol. 7.
11. R. J. Speedy, J. Phys. Chem. 86, 982 (1982).
12. L. Bosio, J. Teixeira, and H. E. Stanley, Phys. Rev. Lett. 46, 597 (1981).
13. H. Kanno, R. J. Speedy, and C. A. Angell, Science 189, 880 (1975).
14. H. Eugene Stanley and J. Teixeira, J. Chem. Phys. 73, 3404 (1980).
15. F. Franks and D. S. Reid in Water, A Comprehensive Treatise, F. Franks, Ed. (Plenum, New York, 1973) Vol. 2.
16. H. D. Bale, R. E. Shepler, and D. K. Sorgen, Phys. Chem. Liquids 1, 181 (1968).

17. M. J. Blandamer in Water, A Comprehensive Treatise, F. Franks, Ed. (Plenum, New York, 1973) Vol. 2.

18. K. Iwasaki and T. Fujiyama, J. Phys. Chem. 81, 1908 (1977).

19. B. Berne and R. Pecora, Dynamic Light Scattering, (John Wiley and Sons, New York, 1976).

20. B. Chu, Laser Light Scattering, (Academic Press, New York, 1974).

21. N. A. Clark, J. H. Lunacek, and G. B. Benedek, Am. J. Phys. 38, 575 (1970).

22. H. Z. Cummins in Photon Correlation and Light Beating Spectroscopy, H. Z. Cummins and E. R. Pike, Ed. (Plenum Press, New York, 1974).

23. K. Iwasaki and T. Fujiyama, J. Phys. Chem. 83, 463 (1979).

24. A. C. Melissinos, Experiments in Modern Physics, (Academic Press, New York, 1966).

25. C.R.C. Handbook of Chemistry and Physics, 57th Edition, Edited by R. C. Weast (C.R.C. Press, Cleveland, Ohio, 1977).

PHOTON CORRELATION SPECTROSCOPY STUDIES OF MUTUAL DIFFUSION IN AQUEOUS t-BUTYL ALCOHOL

by

GARY W. EULISS

B.S., Southwest Missouri State University, 1980

AN ABSTRACT OF A MASTER'S THESIS

submitted in partial fulfillment of the

requirements for the degree

MASTER OF SCIENCE

Department of Physics

KANSAS STATE UNIVERSITY
Manhattan, Kansas

1983

ABSTRACT

In order to study the temporal behavior of the concentration fluctuations in solutions of t-butyl alcohol and water, the mutual diffusion constant in these solutions was measured using photon correlation spectroscopy. The concentration of solutions studied varied from $X_{TBA} = 0.0725$ to $X_{TBA} = 0.260$. Measurements were made from approximately 90°C down into the supercooled regime to approximately -15°C. The viscosity of each solution was then measured. A Stokes-Einstein model was used to analyze the results. This produced correlation lengths of the concentration fluctuations between 5 Å and 10 Å. At high temperatures, the correlation length decreased with decreasing temperature. However, at low temperatures the correlation length increased with decreasing temperature. The high temperature behavior was explained using the idea of a lower critical solution temperature, indicating a second-order phase transition somewhere above the equilibrium boiling temperature. The unique hydrogen bonded structure of the liquid is believed to have been the cause of the low temperature behavior. A liquid clathrate model has been used to explain the nature of this unique structure. A singularity in the correlation length at some lower temperature was inferred by the results. This singularity was interpreted in terms of its relationship to the limit of stability in supercooled water.